Natural Resources Canada | Ressources naturelles Canada

GEOLOGICAL SURVEY OF CANADA
OPEN FILE 9167

Metal(loid) loadings in drainage from No. 98 shaft, Nipissing mine, Cobalt, Ontario

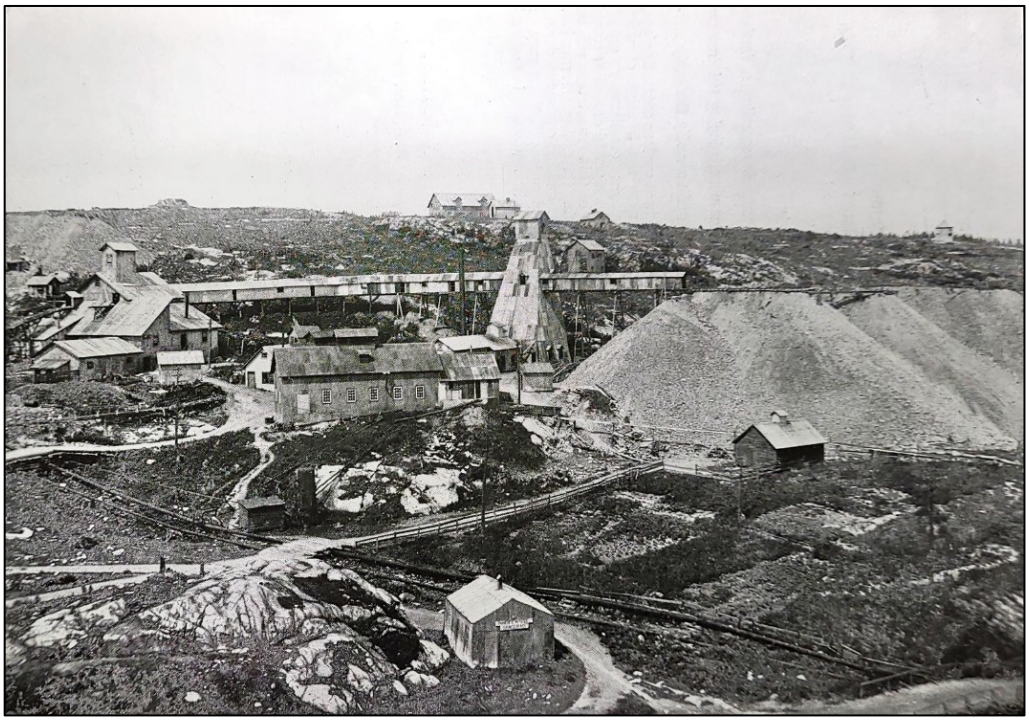

A.J. Desbarats and A. Story

2024

Canada

GEOLOGICAL SURVEY OF CANADA
OPEN FILE 9167

Metal(loid) loadings in drainage from No. 98 shaft, Nipissing mine, Cobalt, Ontario

A.J. Desbarats[1] and A. Story[2]

[1]Geological Survey of Canada, 601 Booth Street, Ottawa, Ontario
[2]Story Environmental and Geomatics, 332 Main Street, Haileybury, Ontario

2024

Permanent link: https://doi.org/10.4095/pez3qkdyg3

This publication is available for free download through the NRCan Open Science and Technology Repository (https://ostrnrcan-dostrncan.canada.ca/).

Recommended citation
Desbarats, A.J. and Story, A., 2024. Metal(loid) loadings in drainage from No. 98 shaft, Nipissing mine, Cobalt, Ontario; Geological Survey of Canada, Open File 9167, 1 .zip file. https://doi.org/10.4095/pez3qkdyg3

Publications in this series have not been edited; they are released as submitted by the author.

ISSN 2816-7155
ISBN 978-0-660-70450-0
Catalogue No. M183-2/9167E-PDF

FOREWORD

The current state of environmental assessment practice in Canada is trending toward Regional Strategic Environmental Assessments (RSEA) because of the need to understand and address cumulative environmental effects of resource development within a broader regional context. To date, cumulative effects assessments have been carried out within the scope of individual project-scale impact assessments. This approach has been found unsatisfactory in regions attempting to manage effects of multiple past, present, and future resource development projects. In line with the Government of Canada's updated environmental assessment legislation (Bill C-69), a key priority of the Geological Survey of Canada's 2019-2024 Environmental Geoscience Program (EGP) was the development of scientific knowledge required for cumulative effects assessment. The EGP project entitled "Cumulative effects of resource development in mining impacted watersheds" addresses the need for cumulative effects research through a case study focusing on the historic Cobalt silver mining camp in northeastern Ontario. The Cobalt camp has seen several cycles of mine development over the last century. Although the last silver mine closed in 1989, exploration companies are turning their focus on the camp once again because of strong world-wide demand for non-conflict cobalt as an essential component of rechargeable batteries used in electric vehicles, consumer electronics, and large-scale storage devices for renewable energy. However, environmental impact assessments of new resource development in watersheds draining the Cobalt area need to take into consideration the cumulative effects of past mining. This report presents monitoring results on the quantity and quality of drainage flowing from a mine shaft in the Cobalt camp. The drainage represents a point source of metal(loids) discharging to the Farr Creek watershed which has been affected by the cumulative impacts of 90 years of mining activity.

Cover photograph: General view of the Nipissing mine north of Cobalt Lake circa 1922 from Knight (1924). Digital collection of the Cobalt Historical Society. Used with permission.

SUMMARY

A monitoring study was conducted on drainage discharging from No. 98 Shaft of the former Nipissing Mine, in Cobalt, Ontario. This drainage represents a point source of metal(loid)s potentially affecting water quality in the downstream receiving environment. Flow rates from the shaft were measured using an H-type flume coupled with a data logger recording water levels. Flow rates were calculated from stage values using a rating equation. Monitoring of flow on an hourly basis lasted from January 21, 2021, to February 3, 2023. Sampling of drainage chemistry on a quasi-weekly basis started on November 24, 2021, and ended on December 7, 2022, for a total of 52 sampling days. Field parameters (EC, pH, DO, ORP, temperature) were measured in the flume at the time of sampling. Mine water chemistry was analysed by the Geological Survey of Canada for a full suite of major, minor, and trace constituents. Combined, these two data sets provide a detailed physical and chemical temporal characterization of drainage from the Shaft 98 hydrogeological system.

During the two-year period of monitoring discharge from Shaft 98, flows varied between 2.1 and 45.4 L/s. The highest flows were observed during the spring freshet, which begins in mid-March and tails off in May. The lowest flows occurred in late summer and early fall, at the end of the hydrological year. Spikes of high discharge were associated with summer convective storms (35 L/s) and late fall rain events (18 L/s). The median flow rate was 6 L/s, and the 95th percentile was approximately 25 L/s.

The drainage from Shaft 98 is a circum-neutral (mean pH=7.1) and sub-oxic (mean DO=1.9 mg/L) Ca-HCO_3 type water with moderate dissolved solids content (mean EC = 392 µS/cm). Water stable isotope analyses fall on the local meteoric water line. The drainage has a mean hardness of 188 mg/L $CaCO_3$. Mean sulfate, nitrate, and chloride concentrations are 17.5, 0.87, and 8.4 mg/L, respectively. Mean dissolved and total Fe concentrations are 55.5 and 130.7 µg/L, respectively. Arsenic (mean dissolved 745.2 µg/L) is the most important metalloid in the drainage. Mean concentrations of dissolved Co, Ni, Sb, and Zn are 98.4, 75.9, 42.2, and 54.3 µg/L , respectively. Annual metal(loid) loadings in drainage from Shaft 98 are estimated at 244.4, 30.0, 22.3, 12.7 and 16.9 kg for As, Co, Ni, Sb, and Zn, respectively. Arsenic, Co, and Ni are mobilized by infiltrating recharge waters through the dissolution of secondary arsenate minerals formed subaerially on exposed walls of the mine workings. Sorption of As on hydrous ferric oxides (HFO) is limited and most As is transported to the Shaft 98 discharge point in dissolved form. Cobalt, Ni, and Sb in mine waters are transported entirely in the dissolved phase.

Overall, the drainage from Shaft 98 exhibits a remarkably “chemostatic” behaviour, meaning that solute concentrations vary little as a function of discharge rate. Nonetheless, some metal(loid) constituents (As, Co, Sb) show subtle “flushing” (increasing concentrations) with increasing discharge rates whereas others (Ni) show “dilution” (decreasing concentrations).

TABLE OF CONTENTS

1. INTRODUCTION

1.1 Background

Exploration for mineral resources, whether for technology-critical elements or traditional commodities, often begins in former mining camps because "the best place to find a new mine is in the shadow of an old mine." Increasingly, companies are also taking a closer look at historical mine wastes, which were formerly considered a liability or too difficult to reprocess, as potential new sources of critical metals (Lottermoser, 2011). These trends in natural resource development highlight the need for environmental impact assessments to consider the cumulative nature of anthropogenic impacts in established mining camps at a broader regional or watershed scale. In the historic Cobalt camp of northeastern Ontario, successive waves of silver mining and milling activity have impacted the Farr Creek watershed with elevated levels of metals and metalloids in soils, sediments, and waters. The prospect of renewed exploration activity for cobalt, with possible new mine development and re-processing of old mine wastes within the watershed, raises concerns about cumulative environmental impacts.

In the Farr Creek catchment, water quality has been affected by the unregulated past disposal of tailings in lakes and by ongoing uncontrolled localized discharge of mine waters. Before assessing potential environmental impacts of new mining development on water quality, it is necessary to identify and characterize both distributed and point sources responsible for the present "brownfield" baseline of pervasive metal(loid) contamination within the catchment. Attribution of contaminant sources, and their relative contribution to overall loadings in the catchment, provides insight into their longer-term evolution in the context of cumulative effects assessment.

Discharge from No. 98 Shaft of the historical Nipissing mine represents a perennial point source of metal(loid) loadings to the Farr Creek catchment. This report presents results from continuous monitoring of drainage flow rate and quasi-weekly sampling of its chemistry. These results will allow researchers to investigate physical and geochemical processes controlling the mobilization and export of metal(loid)s from mine workings. They may be used to analyze possible trend directions in contaminant loadings due to a changing climate and the depletion of reactive source minerals. This includes the response of mine water concentrations and loadings to extreme precipitation or snowmelt events, or extended periods of drought related to climate change.

1.2 The Nipissing Mines Company Ltd.

In terms of total silver production and extent of underground development, the Nipissing Mines Company Ltd. was the most important operator in the Cobalt camp. To the end of 1922, the company had produced 65,700,579 troy ounces of silver and opened 28.2 miles (45.4 km) of drifts, crosscuts, winzes, and shafts across their various properties (Knight, 1924). On their property northwest of Cobalt Lake (RL400), the interconnected workings of the Nipissing Mines Company consisted of (Sergiades, 1968):

- Shaft No. 64, sunk to 902' (275 m) with winze to 1002' (305 m), and 7 levels.
- Shaft No. 73, sunk to 328' (100 m) with winze to 548' (167 m), and 6 levels.

- Shaft No. 98, sunk to 333’ (101 m).
- Shaft No. 80, sunk to 191’ (58 m) with winze to 373’ (114 m).
- Promise Shaft, sunk to 104’ (32 m).

Most production came from four main vein systems (Knight, 1924; Sergiades, 1968):

1. No. 64 vein system, representing the eastward extension of veins on the adjacent Hudson Bay property. It is hosted by an east-striking fault and yielded more than 10 million oz. of silver.
2. No. 80 and No. 100 vein system, representing the eastward extension of veins on the Coniagas property.
3. No. 490 vein system, striking north and south on the east side of the Nipissing property. It is estimated to have yielded several million ounces of silver.
4. No. 73 (Meyer) vein system, representing the eastward extension of the “Main” vein on the Trethewey property. Silver production from the Meyer vein was estimated at 13 million oz. The No. 98 vein, accessed by No. 98 Shaft, is the main branch of the Meyer vein, and it yielded approximately 4 million oz. of silver.

Level plans of the workings showing these vein systems can be found on sheet no. 31a-11 of Knight (1924). Figure 1, reproduced from Knight (1924), shows the extent of workings of the 4th level of the Nipissing mine including the location of No. 98 Shaft. These workings connect the shaft with large open cuts on the surface of the neighbouring Trethewey and Coniagas properties.

1.3 Objectives and Scope

Artesian discharge of mine water from No. 98 Shaft of the former Nipissing mine represents a point source of metal and metalloid loading to the Farr Creek watershed. The objectives of this study are to characterize temporal variations in the quantity and quality of the discharge on a daily, seasonal, and yearly basis with a view to understanding the physical and chemical processes controlling the export of metal(loid)s to the receiving environment. Specific questions to be addressed include:

1. How does the quantity of mine drainage vary in response to snowmelt and precipitation events?
2. What are the geochemical characteristics of mine drainage?
3. How does drainage quality vary with discharge rate?
4. What are the annual metal(loid) loadings from No. 98 Shaft?
5. What are the geochemical processes that may control the metal(loid) chemistry of mine drainage?

The scope of this report is limited to a presentation and preliminary interpretation of flow and aqueous chemistry results from monitoring at the No. 98 Shaft. The data sets accompanying this report will allow researchers to investigate relationships between concentrations of metal(loids) and discharge rates from mine sources under evolving climatic conditions. These relationships are important for understanding the interplay between solute reactions and transport from the workings, as well as for developing practical methods for estimating metal(loid) loadings to the environment.

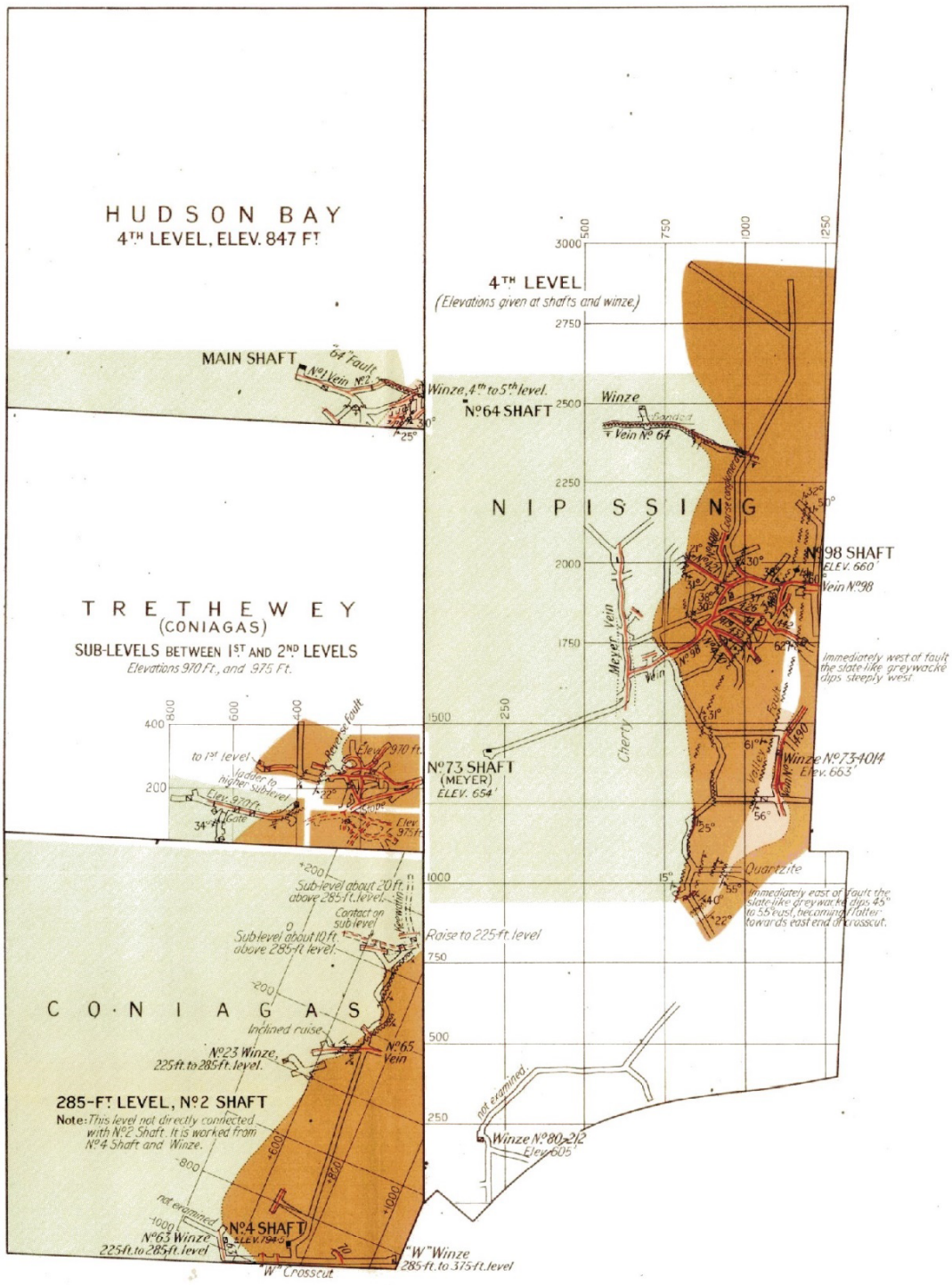

Figure 1: Map showing the 4th Level of the Nipissing Mines property northwest of Cobalt Lake and the location of No.98 Shaft (lat. 47.403°; lon. 79.681° W). Rocks of the Gowganda member of the Cobalt Group are shown in brown. Archean volcanics are shown in pale green. Reproduced from Sheet 31a-11 of Knight (1924). Original scale of 400 ft to 1 inch.

1.4 Accompanying Data Files

This report is accompanied by two data files in Microsoft Excel® format. The files are described as follows:

- of_9167_Drainage_Flow.xlsx: file containing data logger records from the flume.
- of_9167_Drainage_Chemistry.xlsx: file containing analytical results for drainage chemistry.

1.5 Acknowledgments

This project was funded by the Environmental Geosciences Program of the Geological Survey of Canada. The authors gratefully acknowledge Agnico Eagle Mines for permission to carry out this study on their property. Mine water chemistry analyses were performed by Pierre Pelchat and John Sekerka under the supervision of Paul Gammon. The authors acknowledge the contributions of April James (Nipissing University) and Krys Chutko (now at University of Saskatchewan) for providing the stable water isotope data from 2014-2016 used to develop the local meteoric water line cited in this study. Maggie Wilson of the Cobalt Historical Society graciously authorized our use of the photograph on the front cover. The authors would like to thank Melissa Bunn, Ken Korman, and Josée Brazeau for providing helpful comments on earlier drafts of this report.

2. STUDY AREA

2.1 Climatic and Physiographic Setting

No. 98 Shaft of the former Nipissing Mine (lat. 47.403°; lon. 79.681° W) is located in the town of Cobalt (population 989, 2021 census), in the Timiskaming District of Northern Ontario. Cobalt is approximately 500 km northwest of Ottawa and is accessed from the National Capital region via highways 17, 11, and 11B.

The study area falls within the “Humid Low Boreal” (LBh) ecoclimatic region, which is characterized by warm summers and cold winters (EWG, 1989). At Environment Canada’s Ville Marie weather station (discontinued), 19 km southeast of Cobalt, the annual mean daily temperature is 3.1 °C. Mean daily summer (July) and winter (January) temperatures are 18.3°C and -15 °C, respectively. Mean annual precipitation is approximately 837 mm including 656 mm of rainfall and 181 mm of snowfall equivalent. At Earlton Airport, 36 km north-northwest of Cobalt and the nearest active weather station, the annual mean daily temperature is 2.6 °C. The mean daily summer (July) and winter (January) temperatures are 18.3°C and -16.2 °C, respectively. Mean annual precipitation is 786 mm including 576 mm of rainfall and 222 cm of snowfall. Climate Normals (1981-2010) for the Ville Marie and Earlton weathers station are presented in Tables 1 and 2, respectively.

Drainage from No. 98 Shaft flows to Sasaginaga Creek, an upstream tributary of Farr Creek. Most of the mining-impacted areas of the Cobalt camp are in the catchment of Farr Creek, which empties into Lake Timiskaming. Summary hydrometric data for Farr Creek are given in Table 3. The daily hydrograph for a typical year (1980) is dominated by the spring freshet (Figure 2).

Table 1: Climate Normals (1981-2010) for weather station (7088760) at Ville Marie, Québec (lat. 47° 21.00', lon. 79° 26.00' W, elevation 213 m). Data from ECCC (2023).

Month	Daily Average Temperature (°C)	Daily Maximum Temperature (°C)	Daily Minimum Temperature (°C)	Rainfall (mm)	Snowfall (cm)	Precipitation (mm)
Jan	-15.0	-8.7	-21.3	11.5	39.8	51.4
Feb	-12.8	-6.2	-19.5	4.6	31.1	35.8
Mar	-6.4	-0.2	-12.6	18.7	31.2	49.9
Apr	2.9	9.0	-3.3	44.8	13.2	58.0
May	10.5	17.3	3.7	78.4	0.2	78.6
Jun	15.7	22.3	9.1	89.9	0	89.9
Jul	18.3	24.6	12.0	87.7	0	87.7
Aug	17.1	23.2	11.1	96.4	0	96.4
Sep	12.3	17.5	7.0	85.4	0	85.4
Oct	6.0	10.5	1.3	85.2	3.4	88.6
Nov	-1.8	2.0	-5.6	41.3	23.2	64.5
Dec	-9.6	-4.6	-14.7	12.1	38.4	50.4
Year	**3.1**	**8.9**	**-2.7**	**656**	**181**	**837**

Table 2: Climate Normals (1981-2010) for weather station (6072225) at Earlton Airport, Ontario (lat. 47° 42.00', lon. 79° 51.00' W, elevation 243 m). Data from ECCC (2023).

Month	Daily Average Temperature (°C)	Daily Maximum Temperature (°C)	Daily Minimum Temperature (°C)	Rainfall (mm)	Snowfall (cm)	Precipitation (mm)
Jan	-16.2	-10.0	-22.4	4.2	46.9	47.2
Feb	-13.3	-6.5	-20.1	3.4	38.3	39.9
Mar	-6.7	-0.5	-12.9	18.0	34.1	50.7
Apr	2.6	8.5	-3.3	39.6	15.7	54.7
May	10.4	17.2	3.5	70.9	1.7	72.7
Jun	15.6	22.3	8.8	79.0	0.2	79.2
Jul	18.3	24.8	11.8	84.4	0	84.4
Aug	16.8	23.2	10.4	80.8	0	80.8
Sep	12..0	17.9	6.1	86.5	0.3	86.7
Oct	5.1	10.0	0.3	70.0	5.6	75.6
Nov	-2.7	1.4	-6.7	30.6	34.8	63.8
Dec	-10.9	-5.8	-16.0	9.3	44.8	50.5
Year	**2.6**	**8.5**	**-3.4**	**576**	**222**	**786**

Cobalt is situated in the Lake Timiskaming Lowland ecoregion, within the much broader Boreal Shield ecozone (ESWG, 1995). The ecoregion is generally underlain by Precambrian volcanic and intrusive bedrock, forming hummocky and undulating, broadly sloping uplands, and lowlands. Locally, the Cobalt Plain is underlain by flat-lying Proterozoic clastic sediments with ridges and hills formed by diabase sills or granitic rock inliers. Elevations range between 384 m on the summit of Diabase Hill and 178 m on Lake Timiskaming. The area is mantled by glacial till increasing in thickness southward. Bedrock outcroppings are common, and Humo-Ferric Podzols developed on discontinuous sandy glacio-fluvial and outwash deposits are the dominant soil type. A large area of fine-textured glacio-lacustrine deposits occurs around New Liskeard and forms the Gleysolic soils of the Little Clay Belt. The mixed forest of the ecoregion is characterized by white spruce, balsam fir, and eastern white pine, along with some red pine, yellow birch, and trembling aspen. Warmer areas may host sugar and red maple, and yellow birch, whereas white, red, and jack pine

occur on drier terrain. Black spruce, tamarack, and eastern white cedar dominate growth in poorly drained areas. Characteristic wildlife includes moose, black bear, lynx, snowshoe hare, wolf, coyote, and white-tailed deer. Bird species include the American black duck, wood duck, hooded merganser, and pileated woodpecker (ESWG, 1995). Major land uses include forestry, mining, hydroelectric power generation (on the Montreal River), and recreation. The Little Clay Belt of New Liskeard supports livestock and grain farming. Although no mines are currently in operation, the landscape of the Cobalt area has been extensively modified by almost ninety years of mining activity (Dumaresq, 1993; 2023). Because of its colourful mining past and key importance in the development of hard-rock mining in Canada, Cobalt has been named Ontario's Most Historic Town and designated a Parks Canada National Historic Site.

Table 3: Average monthly flow rate (m^3/s) measured at WSC Station 02JE018 (discontinued): Farr Creek at North Cobalt (lat. 47° 25' 28", lon. 79° 37' 59" W); Gross drainage area 62.9 km^2; Data from WSC (2023).

YEAR	Jan	Feb	Mar	Apr	May	Jun	Jul	Aug	Sep	Oct	Nov	Dec	Mean
1971	-	-	0.135	2.47	1.68	0.425	0.161	0.086	0.105	0.115	0.211	0.448	-
1972	0.195	0.255	0.201	1.23	3.78	0.452	0.254	0.369	0.314	1.090	1.040	0.395	0.798
1973	0.351	0.303	2.260	2.52	1.76	1.080	0.208	0.176	0.130	0.362	0.477	0.410	0.836
1974	0.198	0.153	0.450	3.28	2.05	0.860	0.619	0.194	0.200	0.659	0.681	0.497	0.820
1975	0.386	0.229	0.279	2.03	2.21	0.713	0.125	0.116	0.054	0.091	0.084	0.319	0.553
1976	0.172	0.128	1.250	2.55	1.69	0.443	0.087	0.062	0.209	0.220	0.206	0.189	0.601
1977	0.176	0.173	0.856	1.63	0.213	0.189	0.090	0.131	0.163	0.292	0.310	0.369	0.383
1978	0.181	0.128	0.119	1.26	2.18	0.459	0.161	0.087	0.203	0.363	0.263	0.262	0.472
1979	0.209	0.164	0.836	4.20	2.17	0.756	0.482	0.214	0.249	0.735	0.711	0.437	0.930
1980	0.297	0.140	0.352	4.03	1.48	0.252	0.117	0.088	0.161	0.553	0.492	0.245	0.684
1981	0.166	0.759	0.902	3.70	0.955	0.646	0.260	0.059	0.129	0.407	0.574	0.460	0.751
1982	0.259	0.219	0.239	2.71	1.09	0.251	0.099	0.049	0.160	0.400	0.480	0.536	0.541
1983	0.337	0.165	0.736	2.65	2.85	0.743	0.167	0.230	0.140	0.319	-	-	-
Mean	0.244	0.235	0.663	2.64	1.85	0.559	0.218	0.143	0.171	0.431	0.461	0.381	0.666
Max	0.386	0.759	2.260	4.20	3.78	1.080	0.619	0.369	0.314	1.090	1.040	0.536	1.370
Min	0.166	0.128	0.119	1.23	0.213	0.189	0.087	0.049	0.054	0.091	0.084	0.189	0.217

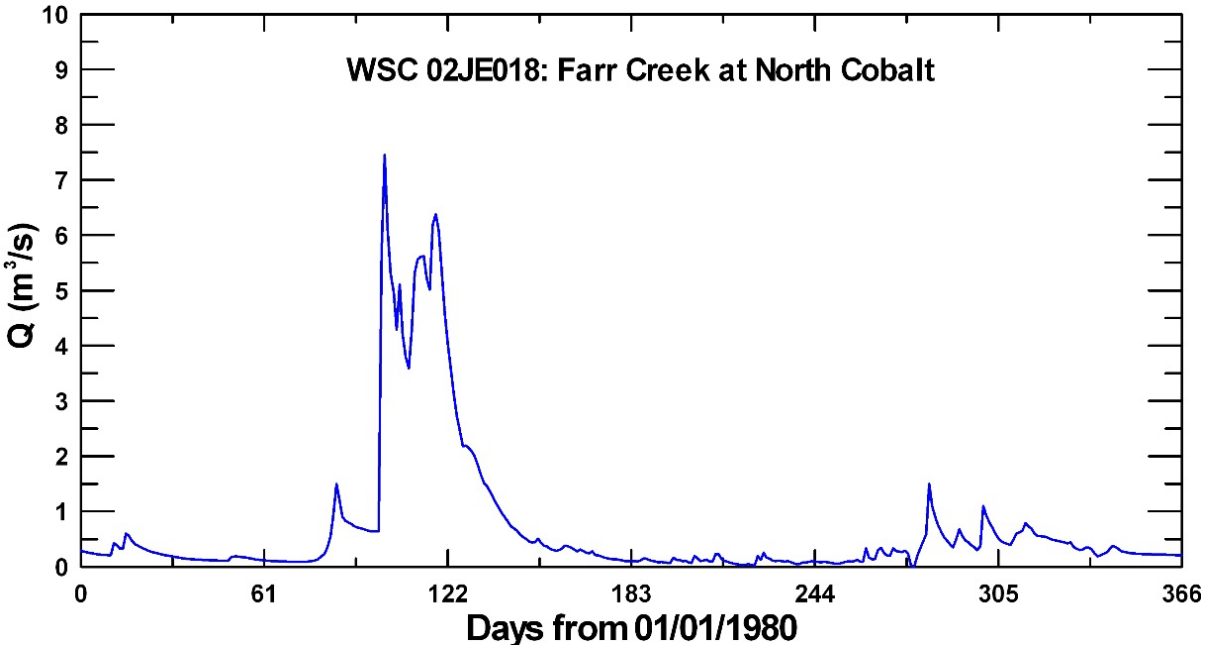

Figure 2: Hydrograph of daily flow rates measured at Water Survey of Canada station 02JE018 during 1980.

2.2 Geological setting

The geology of the Cobalt silver mining camp and the mineralogy of its ores have been described by numerous authors including Miller (1913), Knight (1924), Thomson (1957), and Andrews et al. (1986). However, the most detailed studies can be found in the volume edited by Berry (1971). The following summary draws from these studies including Jambor (1971a; b; c), Petruk (1971a; b), Petruk et al. (1971a; b), and Boyle and Dass (1971).

Except for a small Paleozoic outlier at the north end of Lake Timiskaming, the entire region is underlain by Precambrian rock types with a simple structural configuration. A basement of steeply dipping Archean volcanics is overlain uncomformably by flat-lying Proterozoic sediments. Both lithologies are intruded by undulating sheet-like sills of diabase.

The Archean rocks consist of tightly folded mafic to intermediate flows with intercalated beds of sediments and pyroclastics. The flows are massive to pillow form. Interflow rocks are made up of chert, tuff, and greywacke, and are often mineralized in pyrite, pyrrhotite, chalcopyrite, sphalerite, and galena. The surface of the post-Archean unconformity exhibits significant relief with erosional valleys preferentially occurring above softer interflow rocks. Relatively undeformed, green-schist facies sediments of the Proterozoic ("Huronian") Cobalt Group rest on the unconformity. In the study area, the Cobalt Group is represented by two formations, the Gowganda and the overlying Lorrain. The Gowganda Formation, of glacial origin, has been further subdivided into the basal Coleman and upper Firstbrook members. The Coleman member consists mainly of conglomerate (tillite) with horizons of argillite, arkose, and quartzite. It approaches its maximum

thickness of about 180 m in erosional valleys above the unconformity. The 210-305 m thick Firstbrook member consists of thin, well-bedded, alternating layers of reddish, greenish, or greyish greywackes and argillites. The overlying Lorrain Formation is the most frequently exposed rock in the study area although its upper part has been removed by erosion. It typically consists of pinkish arkoses grading upwards into greenish quartzites. Where the Gowganda Formation is absent or eroded away, the Lorrain Formation rests directly on the Archean basement. Elsewhere, the contact between the Gowganda and Lorrain Formations appears gradational.

While there are a few major faults in the region, the flat-lying attitude of the Proterozoic sediments indicates a relatively stable tectonic environment since their deposition. However, the Huronian and older rocks have been intruded by regionally extensive sills of tholeiitic diabase. These massive (circa 2219 Ma) intrusions, known as the "Nipissing diabase", have an estimated maximum thickness of 335 m in the study area. The plane of intrusion does not appear to have been controlled by either sedimentary bedding in the Huronian or the Archean unconformity. Undulations in the diabase sheets produced a series of basins and domes or arches. The higher features have been removed by erosion while the lower parts have been preserved as isolated basins. Ore veins are either hosted by the diabase itself or by Huronian and Archean country rocks close below or above the diabase contacts. Veins above the diabase and in its upper part occur within basin structures while those below the diabase or in its lower part are under dome structures. Vertical proximity to the Nipissing diabase is recognized as an essential control on the occurrence of silver mineralization in the Cobalt mining camp.

2.3 Economic geology and mineralogy

The bonanza-grade Ag deposits in the study area northwest of Cobalt Lake occur within steeply dipping veins hosted by fissures, fractures, and faults in sediments of the Huronian Coleman member, near the unconformity with underlying Archean rocks. The veins form networks within east-west trending troughs representing pre-Huronian erosional valleys located above mineralized interflow rocks. Ore shoots within the veins typically extend about 45 m above the Archean contact, which is estimated to be 210 m below the overlying Nipissing diabase now eroded away. Silver grades are highest near the top of the orebodies and decrease towards the contact. The extensions of the veins above the ore shoots contain barren carbonates. Below the Coleman contact with Archean volcanics, the vein material consists of barren carbonates or Co-Fe arsenides. The Meyer vein system is representative of those in the study area as well as one of the most important. It extends over 730 m (2400 ft.) across the Trethewey, Nipissing (RL400 W1/2), and Chambers-Ferland (Alladin, RL400 E1/2) properties (Figure A-1). It contains orebodies with a combined length of 490 m (1600 ft) and average grade of about 3.1 % Ag or 1000 oz/t. The No. 98 vein, accessed by Shaft 98 of the Nipissing mine, represents the main branch of the Meyer vein, and continues to the east before pinching out in the Chambers-Ferland property (Figure 1).

Primary mineralogy of the veins

The ore veins of the Cobalt camp consist of arsenides, native metals, and sulfides, in a gangue of dolomite, calcite, quartz, chlorite, and oxide minerals. A list of metal(loid) vein minerals is provided in Table 4. Nickel, Co, and Fe arsenides are found in distinct mineral assemblages, gradational from one another and distributed systematically across most veins. The zonation of arsenide assemblages

depends on the location of the vein relative to the diabase sill. Below the Nipissing diabase, as in the No. 98 vein, a Ni-As assemblage is typically found at the top of veins. The nickel and arsenide minerals occur as disseminations and masses exhibiting complex textures and intergrowths composed mainly of nickeline, rammelsbergite, breihauptite, cobaltite, and safflorite. The Ni-As assemblage transitions downward to a Ni-Co-As assemblage dominated by nickeline in its upper part. This assemblage becomes dominated by rammelsbergite before grading into a Co-As assemblage. The Co-As assemblage forms the main part of most veins. The arsenide minerals there are found as disseminated grains and massive clusters of zoned rosettes consisting of intergrowths of safflorite, cobaltite, and skutterudite. The lower part of veins is characterized by a Co-Fe-As assemblage dominated by arsenopyrite with lesser amounts of cobaltite, skutterudite, and safflorite. The bottom and tips of the veins are characterized by a Fe-As assemblage consisting mainly of arsenopyrite.

Silver is the most important native metal found in the veins. It is closely associated with the Ni-Co-As and Co-As arsenide assemblages where it occurs at the core of rosette structures. In the nickeline-rich portion of the Ni-Co-As assemblage, native silver is found intergrown with allargentum, an Ag-Sb mineral. Generally, the highest Ag grades are associated with the Ni-Co-As and Co-As assemblages, medium to low grades are found with the Co-As and Co-Fe-As assemblages, and low grades are associated with the Fe-As and Ni-As assemblages. Some native bismuth occurs near the bottom and tips of veins in association with the Co-Fe-As and Fe-As arsenide assemblages.

A wide variety of sulfide minerals are found in the veins (Petruk et al., 1971b). However, the most common are chalcopyrite and tetrahedrite. These minerals occur as disseminated grains and veinlets throughout both barren and highly mineralized portions of the veins. They are sometimes associated with native silver or with bornite, chalcocite, and other sulfides. Galena, sphalerite, marcasite, and pyrite are common in barren veins and within the Fe-As arsenide vein assemblage. Other sulfide minerals include acanthite and pyrargyrite associated with native silver, and bismuthinite associated with native bismuth. Oxide minerals are rare in the veins but include small amounts of hematite, magnetite, rutile, anatase, and ilmenite.

Secondary mineralogy of the veins

Because of glacial erosion and the low-permeability of clay-till overburden, most of the veins in the Cobalt mining camp show little evidence of in-situ weathering beyond thin surficial traces of cobalt and nickel bloom. However, deep weathering of one vein allowed Boyle and Dass (1971) to investigate supergene processes affecting primary ore and gangue minerals. Secondary minerals identified by the authors include limonite, wad (amorphous Mn oxyhydroxides), clays, calcite, erythrite, annabergite, scorodite, melanterite, malachite, and azurite. Erythrite and scorodite are the most abundant arsenates. Chapmanite, a secondary Sb mineral, has also been reported (Walker, 1924). Significant amounts of Co and Ni are adsorbed or co-precipitated with hydrous Fe and Mn oxides along with lesser amounts of Sb and Bi. Copper sulfide minerals weather to malachite and azurite. Galena alters to anglesite. No secondary Zn or Cd minerals were observed although melanterite may contain some Cu and Zn. All four sulfide metals (Cu, Pb, Zn, Cd) are strongly adsorbed or co-precipitated with hydrous Fe and Mn oxides. In their study of Ni-Co arsenide mineralization in underground workings of the Wittichen district of Germany, Markl et al. (2014) observed the formation of secondary erythrite, pharmacolite, picropharmacolite, and various Ca-Mg-Co arsenate minerals. In a recent detailed study of mine tailings in the Cobalt camp, Clarke (2017) identified secondary minerals including erythrite-annabergite solid solutions, amorphous Fe-Co-Ni arsenates, and Fe-Ca arsenates.

Wall rock alteration

Alteration zones bordering veins typically consist of an inner albite-chlorite assemblage progressing outward to calcite-dolomite-epidote and sericite assemblages before reaching unaffected rock (Jambor, 1971c). Some calcite may be present in the albite-chlorite zone and some chlorite is usually present in the carbonate zone. In Archean volcanics and in diabase, a K-feldspar, rather than sericite, alteration zone may have formed. In Huronian sediments, alterations zones are often poorly developed. The maximum total width of the alteration zones is no more than 30 cm and appears to be independent of the width of the ore vein.

Table 4: Most common metal(loid) vein minerals.

Group	Mineral	Ideal Formula
sulpharsenides	arsenopyrite	FeAsS
	cobaltite	CoAsS
	gersdorffite	NiAsS
arsenides	nickeline	NiAs
	rammelsbergite	$NiAs_2$
	safflorite	$(Co,Fe)As_2$
	skutterudite	$CoAs_3$
arsenates	annabergite	$Ni_3(AsO_4)_2{:}8H_2O$
	erythrite	$(Co,Ni)_3(AsO_4)_2{:}8H_2O$
	scorodite	$FeAsO_4{:}2H_2O$
antimonides and sulph-antimonides	breithauptite	NiSb
	pyrargyrite	Ag_3SbS_3
	tetrahedrite	$(Cu,Fe)_{12}Sb_4S_{13}$
sulfides	acanthite	Ag_2S
	bismuthinite	Bi_2S_3
	bornite	Cu_5FeS_4
	chalcocite	Cu_2S
	chalcopyrite	$CuFeS_2$
	galena	PbS
	pyrite / marcassite	FeS_2
	sphalerite	ZnS

3. METHODOLOGY

3.1 Site description

Shaft No. 98 of the historical Nipissing Mine was collared at an elevation of 284 m (933 ft) and sunk to a depth 101 m (333 ft). Its collar elevation is the lowest of any of the nearby shafts (Knight, 1924; Appendix 1, Figure A.2). As a result, mine water from an extensive network of flooded workings discharges to the surface through Shaft 98. The shaft has been capped and flow is directed through a large-diameter corrugated pipe to a settling pond. From there, mine water is channeled to Sasaginaga Creek, a tributary of Farr Creek.

3.2 Flow measurements

The flow rate of mine water discharging from Shaft 98 was monitored continuously using a flume combined with a data logger recording water level. Methods for measuring flow in mining environments are reviewed in various guides including Environment Canada (2001) and US EPA (2001). For conditions at the Shaft 98 site, an "H-Type" flume (Gwinn and Parsons, 1976; Grant and Dawson, 1997; Environment Canada, 2001; US EPA, 2001) was selected as the most appropriate primary flow measurement device. It does not require freeboard for impounded water as with a weir; it is accurate over a wide range of flow rates; and it is self-cleaning of sediment accumulation to some extent. The flume, including a 4-foot approach section and a stilling well, was fabricated locally by New Liskeard Sheet Metal Works using ¼'' steel plate (Figure 3) according to published specifications for a D = 1' H Flume (Grant and Dawson, 1997). The flume was installed at the outlet of the pipe discharging flow from Shaft 98, on the edge of an embankment, which allows free-flow conditions (Figure 4). During winter months, the flume was covered by a plywood sheet.

For "H-type" flumes, the relationship between discharge (Q) and water level or stage (H) in the flume depends on flow conditions (low, transitional, main). The main flow equation is of the form (Gwinn and Parsons; 1976):

$$Q = A\ H^{1.5} + B\ H^{2.5} \quad [1]$$

Where the coefficients A and B are functions of flume geometry (Gwinn and Parsons (1976). However, a general rating curve valid for all flow conditions can be obtained empirically by fitting a polynomial function of H to the tabulated stage-discharge relationship for an H Flume (D = 1') found in handbooks (Grant and Dawson, 1997; Brakensiek et al., 1979; OCF, 2023). For this type and size of flume, discharge (in L/s) and stage (in m) are related by (OCF, 2023):

$$Q = 0.005861587 - 0.26824961\ H^{0.5} + 41.00900793\ H^{1.4} + 933.7209182\ H^{2.5} \quad [2]$$

A secondary flow monitoring device is required to measure and record the stage from which discharge is calculated using the equation above. Here, the selected device was a vented Solinst LevelVent 5 data logger Model 3250 with full scale (FS) of 5 m H_2O, accuracy ± 3mm, and resolution 0.001% FS. The data logger was installed in the stilling well, which is hydraulically connected to a head observation port in the flume. The pressure sensor measures the depth of water

in the stilling well above a fixed reference level. Subtracting this depth from the reference level yields the water stage in the flume from which flow can be calculated using the rating equation.

Recording of discharge flow rate at No. 98 Shaft started on January 21, 2021, and ended February 3, 2023, with the failure of the data logger due to freezing of water in the stilling well.

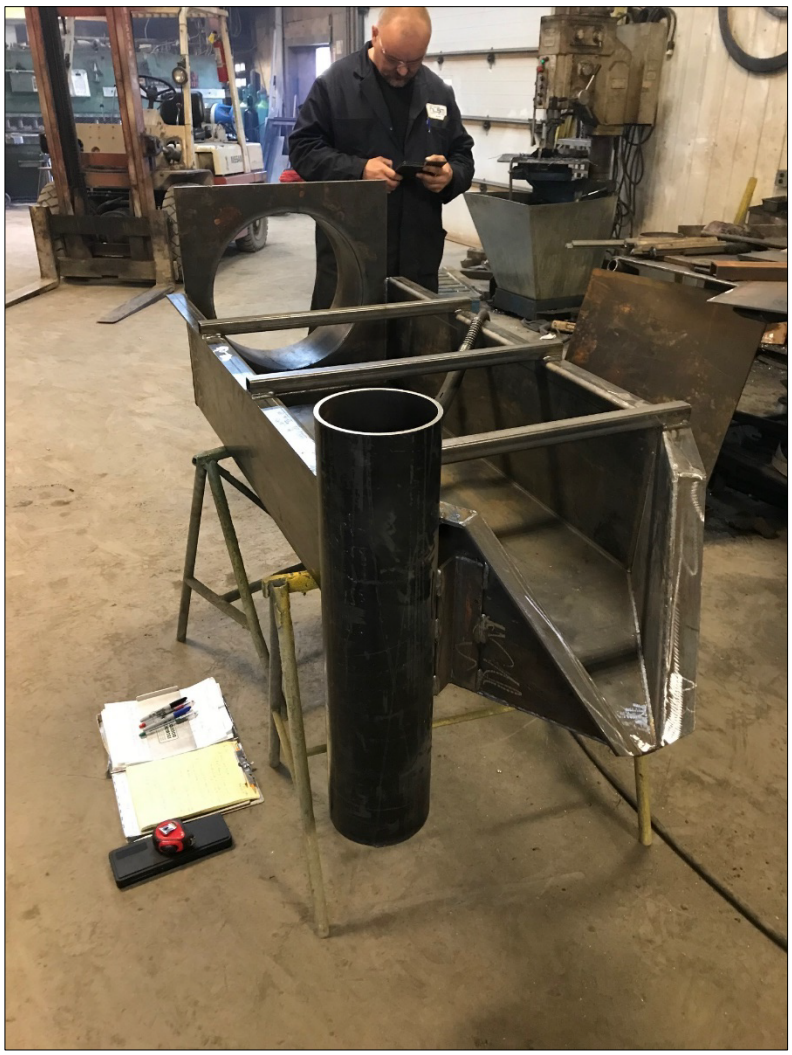

Figure 3: Fabrication of the H Flume by New Liskeard Sheet Metal Works in December 2020. Photograph courtesy of A. Story.

Figure 4: H Flume at the outlet of discharge from Shaft 98 showing data logger in the stilling well. Photograph courtesy of A. Story.

3.2.1 Flow measurement verifications

Verification of the rating curve

For flow rates greater than approximately 1.0 L/s (always the case in this study), the relative error when using [2] to estimate Q from H is less than ± 1% compared to using exact values from the H Flume discharge table (Figure 5).

Verification of data logger stage measurements

During each visit to the site for water sampling, the flume stage was measured manually to check against data logger readings. The precision of manual measurements was typically estimated at ± 5 mm, depending on flow rate and turbulence in the flume. The overall agreement between manual and data logger values is excellent (Figure 6).

Verification of data logger flow rates

Every fourth visit to the site, a manual measurement of flow was taken using the "bucket and stopwatch" method. At high flow rates, this became impractical, and a tracer (NaCl) dilution method (Moore, 2005) was attempted instead. Tracer was added to the flow at the outlet of the corrugated pipe. However, because of the relatively short approach section in the flume, mixing of the tracer was incomplete and this affected flux estimation from the breakthrough curve. Nonetheless, the overall agreement between manually measured flow rates and those calculated from data logger readings using equation 2 is reasonable (Figure 7).

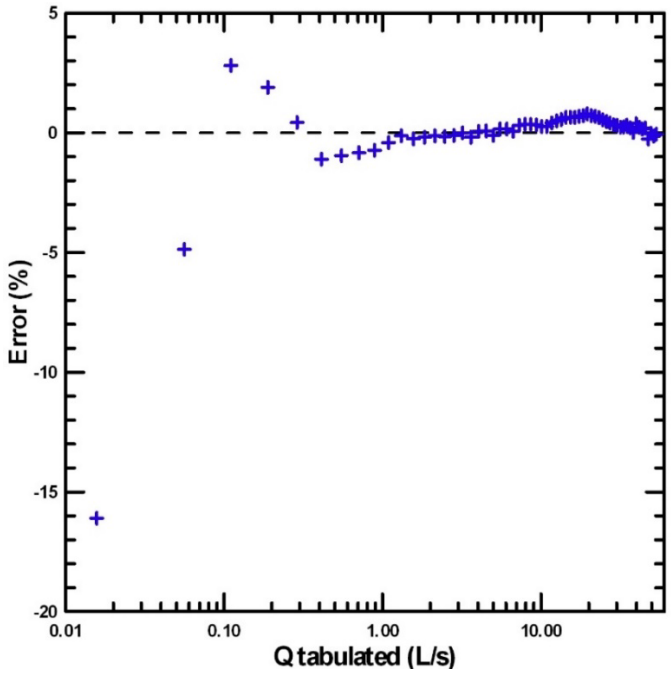

Figure 5: Relative errors when using rating curve [2] to estimate flow rate Q from H versus exact tabulated flow rates from the ISCO Handbook (Grant and Dawson, 1997; OCF, 2023).

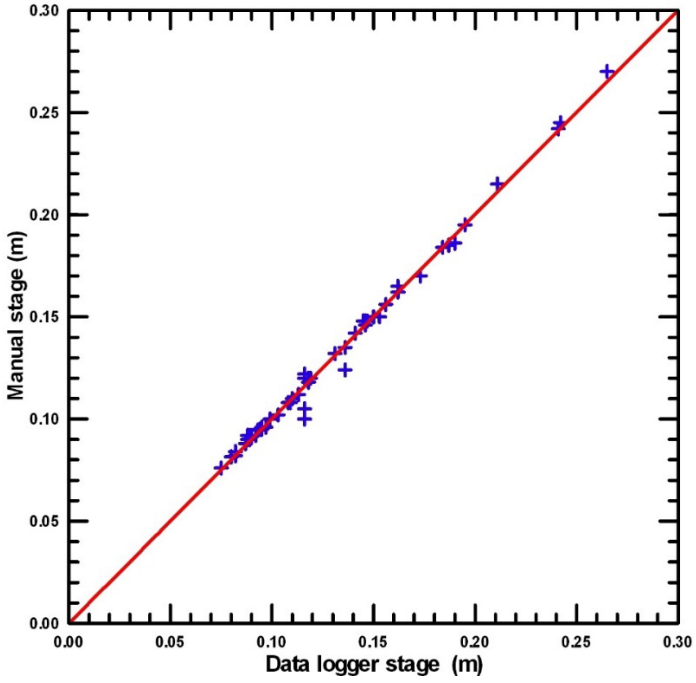

Figure 6: Manual measurements of flume stage versus corresponding values recorded by the data logger.

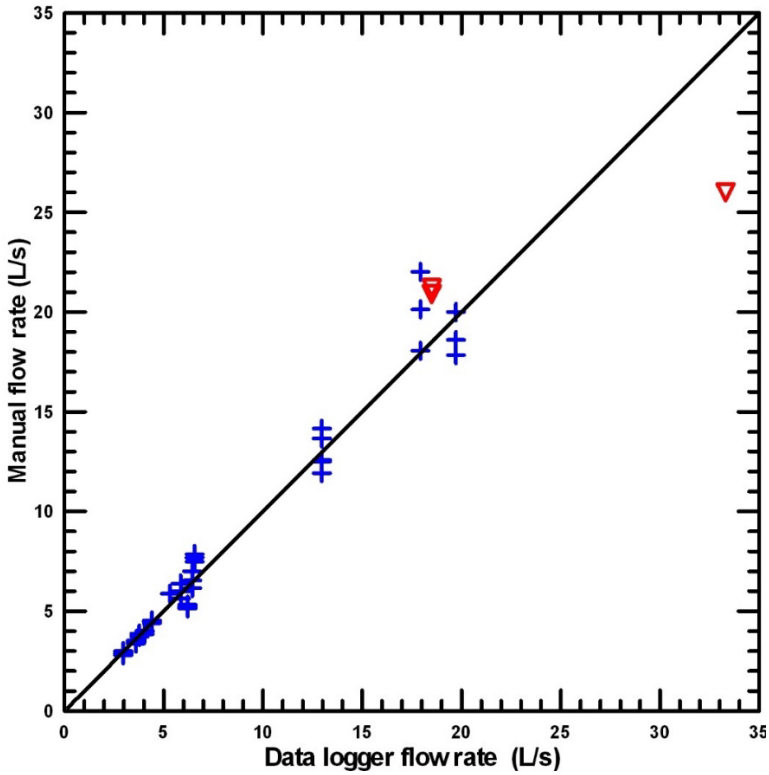

Figure 7: Manual flow measurements versus flow rate calculated from the rating curve using stage values recorded by the data logger. Flow measurements by bucket and stopwatch are indicated by the blue crosses. Measurements obtained by tracer dilution are represented by red triangles.

3.3 Field sampling of drainage chemistry

Measurements of field parameters were made using a YSI Professional Plus™ multiparameter meter calibrated prior to each sampling event. A three-point (4, 7, 10) calibration was used for pH. Calibration for specific conductance was done using a 1000 µS/cm standard (491 mg/L NaCl). The dissolved oxygen probe was calibrated using a one-point DO % water saturated air calibration. The Oxidation-Reduction Potential (ORP) probe was calibrated using a standard ORP solution (+225 mV at 25 °C).

Mine drainage was sampled directly from the flume using all-plastic 50 mL Norm-Ject® syringes triple-rinsed in the water to be sampled. Unfiltered samples for (total) cations were collected in triple-rinsed 60 mL HDPE narrow-mouth bottles (Nalgene® 2002-0002). Filtered (Millipore® Sterivex^{TM} 0.45 µm) samples for anions and cations were collected in 60 mL HDPE narrow-mouth bottles triple-rinsed with filtered water to be sampled. Duplicate water samples and field blanks were collected at every fourth visit to the site. Samples were refrigerated pending monthly shipment of batches to Ottawa. Bottles for cation samples were acidified on arrival at the GSC laboratory in Ottawa. Details of the field sampling protocol are provided in Appendix 2 of this report.

Sampling of drainage chemistry on a quasi-weekly basis started on November 24, 2021, and ended on December 7, 2022, for a total of 52 sampling days.

3.4 Laboratory Methods

All mine water samples were analyzed at the Inorganic Geochemical Research Laboratory of the Geological Survey of Canada in Ottawa. Analyses of major elements were performed by Inductively Coupled Plasma - Atomic Emission Spectroscopy (ICP-AES) using a Perkin-Elmer 3000 DV. Analyses of trace elements were performed using Inductively Coupled Plasma - Mass Spectrometry (ICP-MS) with a Thermo Corporation X-7 Series II. Determinations of anion concentrations were made with a Dionex DX-600 ion chromatograph (IC) using an AS-18 column and gradient elution. Alkalinities were determined by charge balance. Element suites analyzed by each method and their corresponding detection limits are listed in Table 5. For each sample batch, analytical accuracies were checked on two certified standards of known concentrations. Analytical results for field and laboratory blanks from each batch were below detection limits for all elements. Precisions were calculated using the method of Thompson and Howarth (1978). For the major cations (ICP-AES), Ca, Mg, Na, K, and Si, the precisions (± 2 σ) were 0.71 %, 1.24 %, 1.17 %, 1.78 %, and 1.06 %, respectively. For the minor and trace cations (ICP-MS), Fe, Mn, Co, Ni, Cu, Zn, As, and Sb, the precisions (± 2 σ) were 4.12 %, 2.29 %, 1.70 %, 1.19 %, 2.36 %, 1.46 %, 1.52 %, and 1.51 %, respectively. For the anions (IC), Cl, SO_4, and NO_3, the precisions (± 2 σ) were 0.96 %, 1.37 %, and 2.32 %, respectively.

Analyses for stable water isotopes were performed at the Ján Veizer Stable Isotope Laboratory of the University of Ottawa using the Cavity Ring Down System manufactured by Picarro. Precisions for δ^2H and $\delta^{18}O$ were 0.5 ‰ and 1 ‰, respectively. Accuracy was checked using four in-house standards including one blind standard.

Table 5: Analytical methods and corresponding detection limits for elements analyzed.

ICP-MS Element Suite * Lower detection limit in ppb shown in brackets			
Li (0.02)*	Be (0.005)	B (0.5)	Al (1)
Ti (0.1)	V (0.01)	Cr (0.02)	Mn (0.1)
Fe (1)	Co (0.05)	Ni (0.2)	Cu (0.1)
Zn (0.5)	Ga (0.01	Ge (0.02)	As (0.05)
Se (0.05)	Rb (0.05)	Sr (0.5)	Y (0.01)
Zr (0.05)	Nb (0.01)	Mo (0.05)	Ag (0.005)
Cd (0.02)	In (0.01)	Sn (0.01)	Sb (0.01)
Te (0.02)	Cs (0.01)	Ba (0.2)	La (0.002)
Ce (0.002)	Pr (0.001)	Nd (0.001)	Sm (0.001)
Eu (0.001)	Tb (0.001)	Gd (0.001)	Dy (0.001)
Ho (0.001)	Er (0.001)	Tm (0.001)	Yb (0.001)
Lu (0.001)	Hf (0.01)	Ta (0.01)	W (0.02)
Re (0.001)	Tl (0.005)	Pb (0.01)	Bi (0.02)
Th (0.02)	U (0.005)		

ICP-AES Element Suite * Lower detection limit in ppm shown in brackets			
Br (0.05)*	Ca (0.02)	Cl (0.1)	Fe (0.005)
K (0.05)	Mg (0.005)	Na (0.05)	P (0.05)
S (0.05)	Sc (0.001)	Si (0.02)	

IC Element Suite * Lower detection limit in ppm shown in brackets			
F (0.01)*	Cl (0.01)	SO_4 (0.02)	Br (0.02)
NO_3 (0.02)	PO_4 (0.02)		

4. RESULTS

4.1 Physical Hydrogeology

Over the two-year data logging period, mine water discharge rates from Shaft 98 varied between 2.1 and 45.4 L/s, with a median rate of 6 L/s (Table 6). About 5 % of flow rates exceeded 25 L/s (Figure 8). The discharge hydrograph (Figure 9) shows that highest flow rates correspond to the spring freshet, which usually begins when daytime high air temperatures are greater than 0 °C. Isolated high-flow periods are associated with extreme precipitation events, as occurred in June and July of 2021, and with winter thaws, as in December of 2021 (Figure 9). Minimum flows occur in late winter and late summer.

Mine water temperature, as measured in the flume stilling well, varies with air temperature (Figure 10). During winter months, water temperature is usually steady at around than 4 °C. However, during cold snaps, as in February 2021 and 2022, it may dip to below 1 °C. During a very cold period in February of 2023, water in the stilling well froze and the data logger was damaged. There is no obvious relationship between discharge water temperature and precipitation events.

Table 6: Summary statistics for drainage discharge rate.

	Q (L/s)
N	17,842
Minimum	2.1
Maximum	45.4
Median	6.0
Mean	8.8
Std. Dev.	7.0

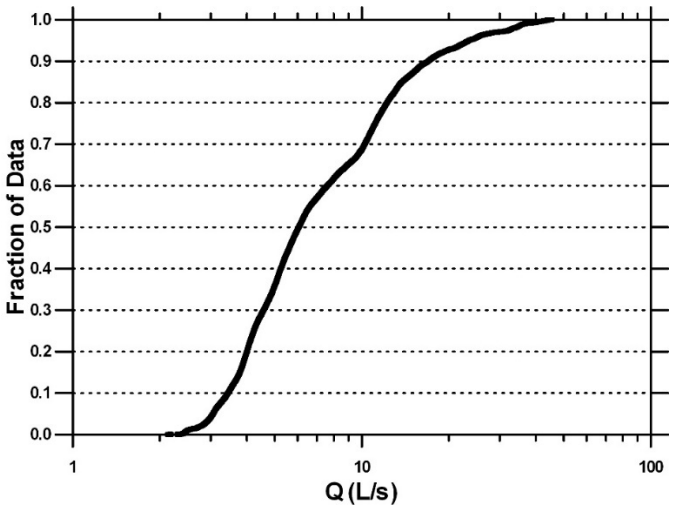

Figure 8: Cumulative distribution function for drainage discharge rate (Q) from Shaft 98 for the full two-year data logging period.

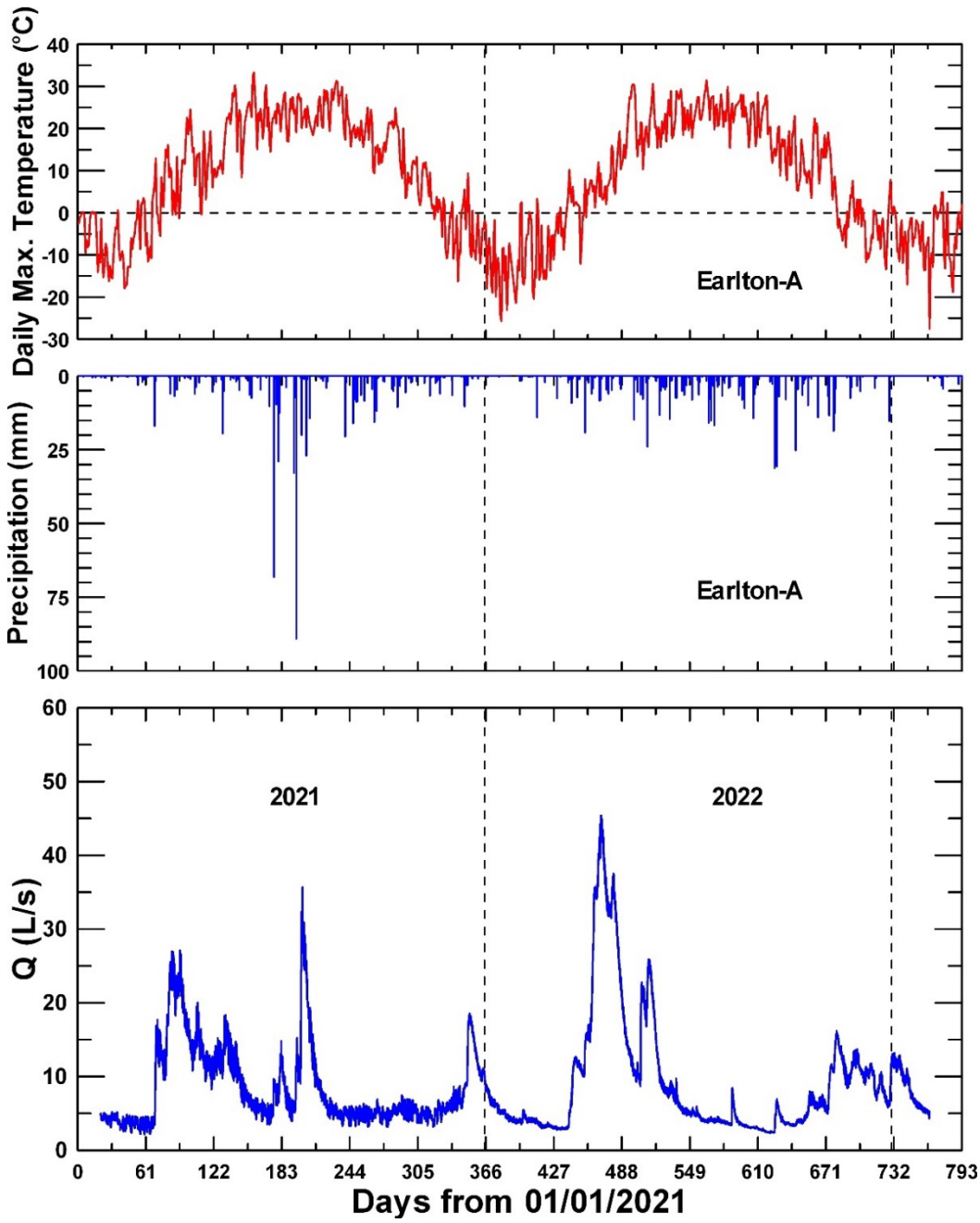

Figure 9: Hydrograph of mine water discharge rate (Q) from Shaft 98 for the full 2-year data logging period. Daily precipitation and maximum temperature at the Earlton-A weather station are shown for reference.

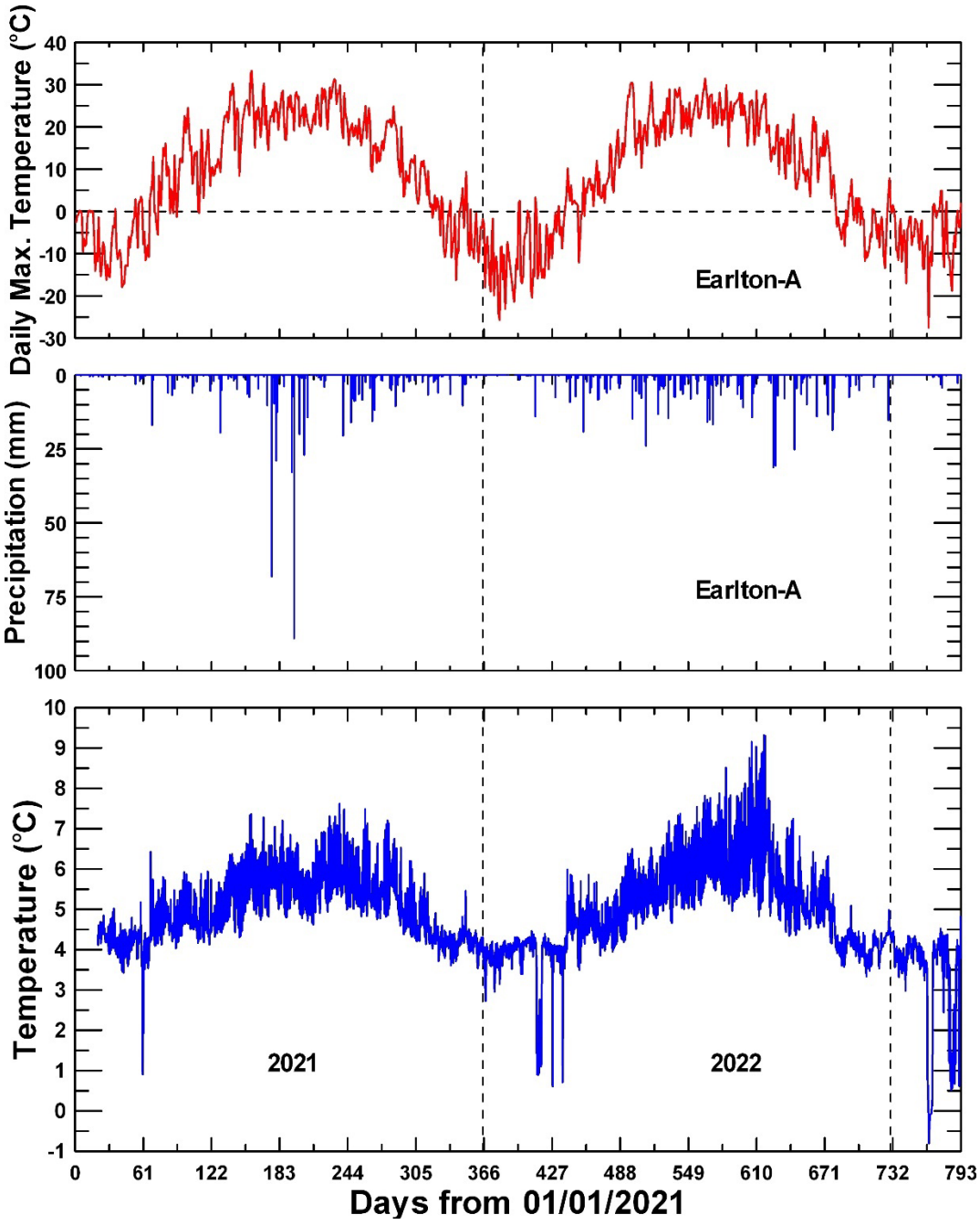

Figure 10: Temperature of mine water discharge from Shaft 98 (as recorded in the flume stilling well) for the full two-year data logging period. Daily precipitation and maximum temperature at the Earlton-A weather station are shown for reference.

4.2 Chemical Hydrogeology

Field Parameters

The pH of mine waters is circum-neutral and varies over a narrow range (Table 7). The temporal pattern of pH variations does not show any clear relationship to discharge rate (Figure 11). The Specific Conductance (SC) of the drainage varies over a narrow range also (Table 7). However, SC shows a gradual increase through the winter of 2022 to a peak following the spring freshet and a decreasing trend over the rest of the year (Figure 12). Dissolved oxygen concentrations (DO) are in the sub-oxic range. They peak during the winter months and decline at the beginning of the spring freshet before gradually recovering (Figure 13). Oxidation-Reduction Potential (ORP) values are highest during the winter and drop sharply during the freshet before recovering over the rest of the year (Figure 14). In May of 2022, at the end of the freshet, ORP values reached a minimum of -28 mV and remained low for the rest of the summer. Mine water temperatures, as measured directly in the discharge stream, are almost constant (Table 7) whereas values measured in the stilling well reflect air temperature variations (Figure 10).

Table 7: Summary statistics for field parameters

	pH	SC µS/cm	DO mg/L	ORP mV	Temp. °C
N	52	52	52	52	52
Minimum	6.78	372.2	1.14	-28.0	4.3
Maximum	7.48	408.3	3.13	279.0	5.1
Median	7.17	391.7	1.79	131.9	4.8
Mean	7.14	391.8	1.86	120.4	4.8
Coeff. Var.	0.02	0.02	0.25	0.78	0.04

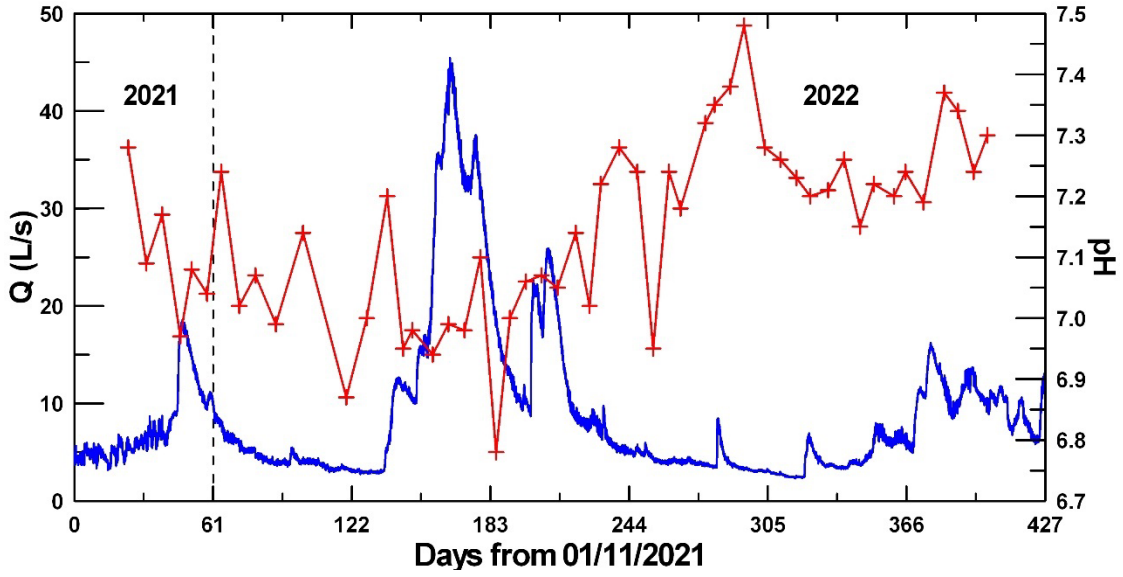

Figure 11: Chemograph of pH (right scale) with overlay of discharge hydrograph (left scale) from November 1, 2021.

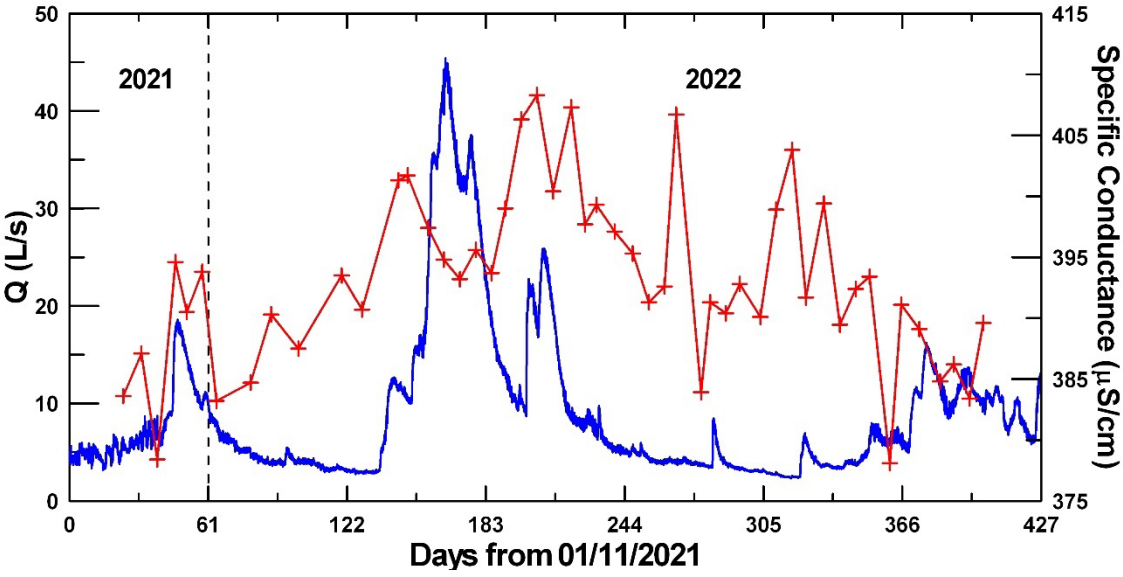

Figure 12: Chemograph of specific conductance (right scale) with overlay of discharge hydrograph (left scale) from November 1, 2021.

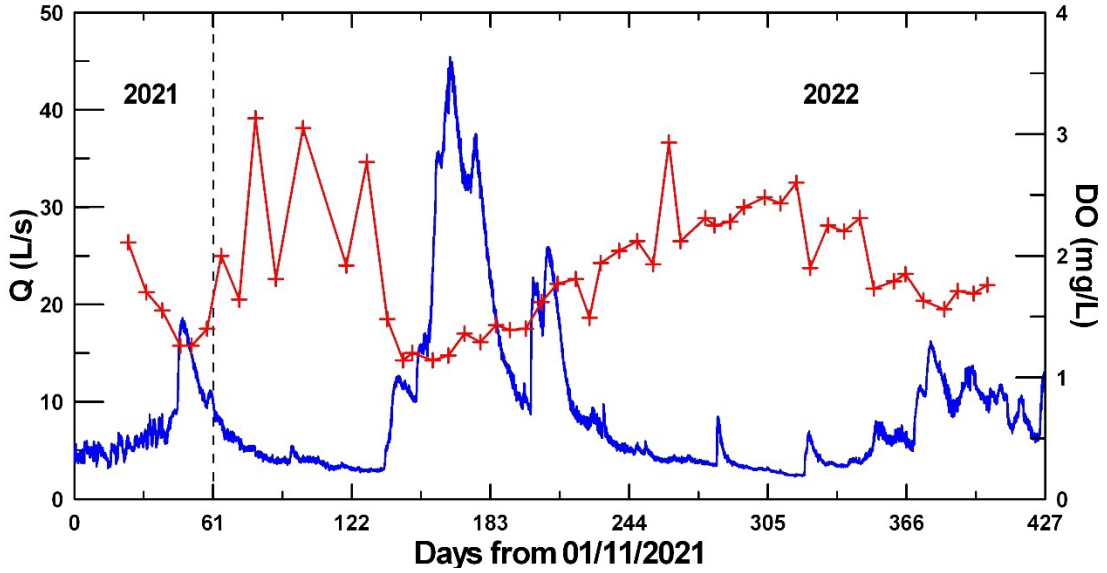

Figure 13: Chemograph of dissolved oxygen (right scale) with overlay of discharge hydrograph (left scale) from November 1, 2021.

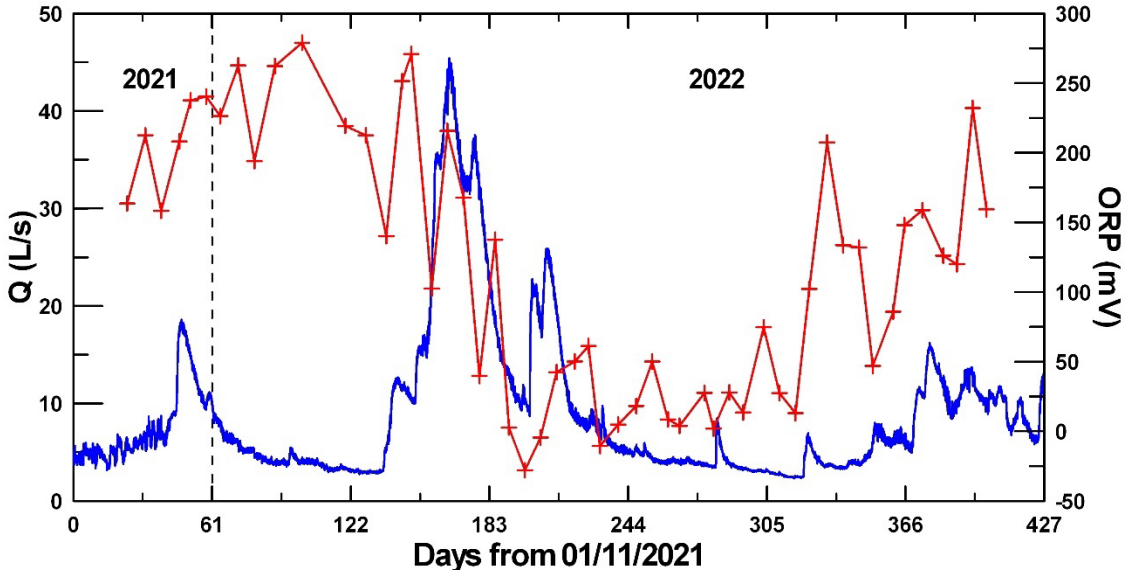

Figure 14: Chemograph of ORP (right scale) with overlay of discharge hydrograph (left scale) from November 1, 2021.

Stable Water Isotopes

Stable water isotope (^{2}H and ^{18}O) concentrations in mine drainage vary over narrow ranges during the study period (Table 8). Values plot on the Local Meteoric Water Line (LMWL) for the Cobalt-Coleman area (Figure 15), as determined by Story Environmental Inc. based on analyses of snow and rain over a two-year period. The isotope data do not suggest any enrichment due to evaporation of recharge waters. Given the linear relationship between $\delta^{2}H$ and $\delta^{18}O$, their patterns of temporal variation are similar (Figures 16 and 17). Both parameters reflect a gradual but slight isotopic enrichment over the winter months before reaching a plateau after the freshet.

Table 8: Summary statistics for stable water isotope concentrations.

	$\delta^{2}H$ (‰)	$\delta^{18}O$ (‰)
N	65	65
Minimum	-91.93	-12.87
Maximum	-89.46	-12.52
Median	-90.07	-12.64
Mean	-90.25	-12.65
Coeff. Var.	-0.007	-0.007

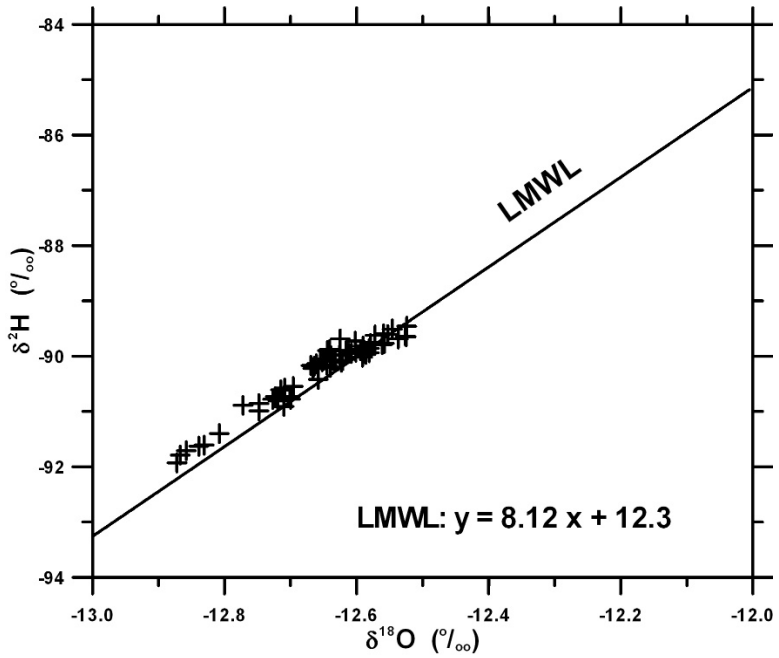

Figure 15: Stable water isotope plot showing the Local Meteoric Water Line (LMWL) obtained by Story Environmental Inc. from snow and rainfall samples over a two-year period (pers. comm.).

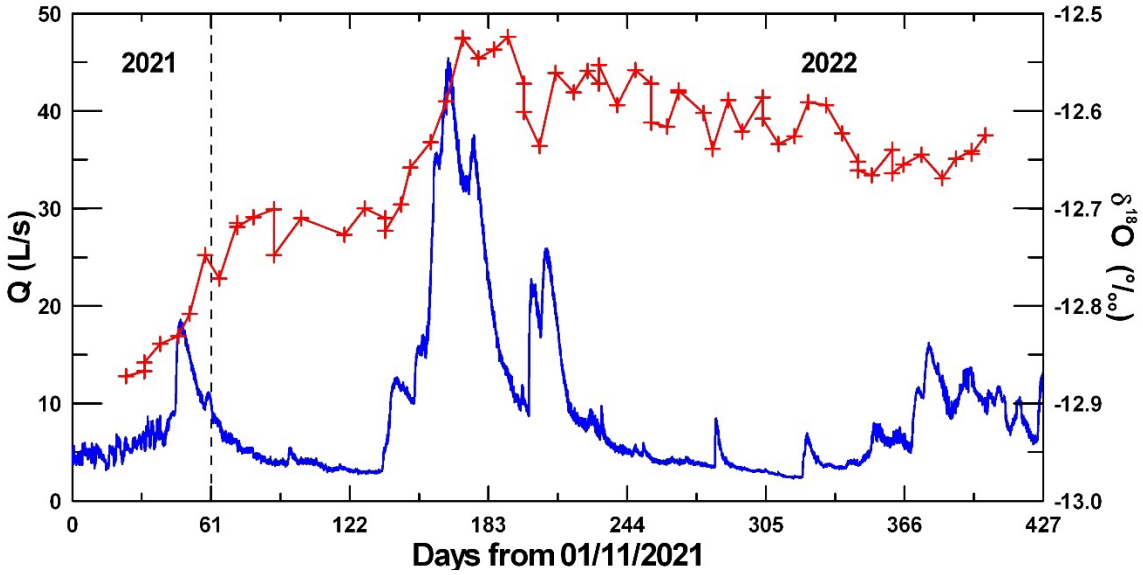

Figure 16: Chemograph of $\delta^{18}O$ (right scale) with overlay of discharge hydrograph (left scale) from November 1, 2021.

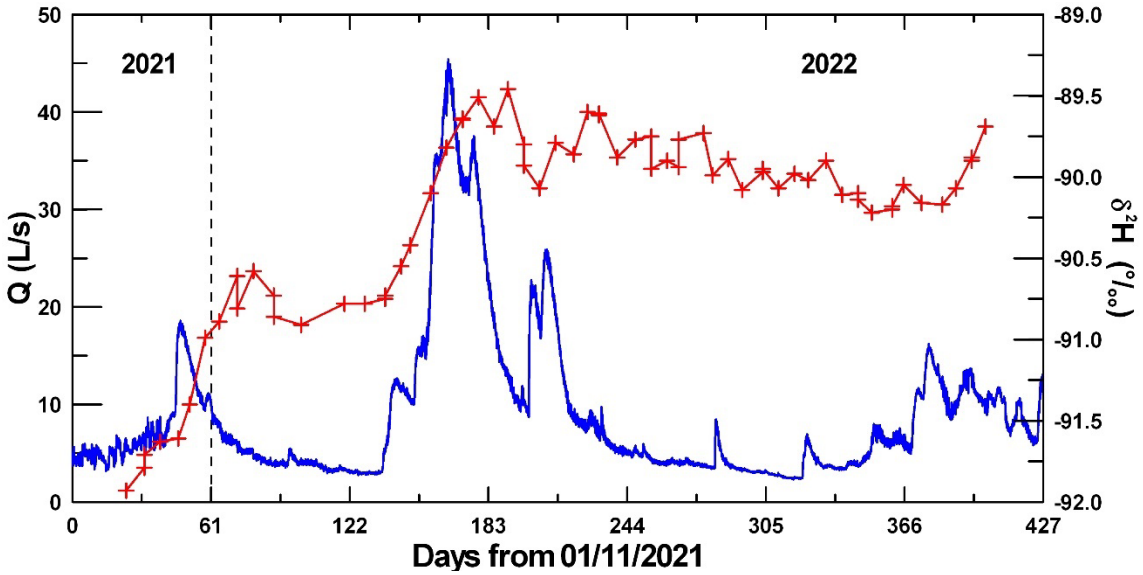

Figure 17: Chemograph of $\delta^{2}H$ (right scale) with overlay of discharge hydrograph (left scale) from November 1, 2021.

Major Cations and Anions

Unless otherwise indicated, reported concentrations are for the "dissolved" phase, from filtered water samples (< 0.45 µm). The most remarkable common characteristic of major cation concentrations is their narrow range of variation during the year-long study (Table 9). The coefficients of variation are only slightly greater than analytical precisions. The chemograph of Ca concentrations exhibits a small peak three months after the freshet but is otherwise featureless (Figure 18). The Mg chemograph shows a dip in concentrations during the freshet followed by an increase before a gradual decline over the rest of the year (Figure 19). Based on Ca and Mg concentrations, mine water from Shaft 98 would be classified as very hard. Temporal variations of Na concentrations show a slight decline following the freshet and then a gradual increase over the fall of 2022 (Figure 20). The chemographs of K and SiO_2 are essentially flat (Figures 21 and 22).

Table 9: Summary statistics for concentrations of major cations.

	Ca (mg/L)	Mg (mg/L)	Hardness (mg/L $CaCO_3$)	Na (mg/L)	K (mg/L)	SiO_2 (mg/L)
N	65	65	65	65	65	65
Minimum	54.872	9.751	177.32	6.316	1.058	7.766
Maximum	61.694	11.123	199.40	7.509	1.201	8.316
Median	57.988	10.410	188.33	6.881	1.122	8.136
Mean	57.884	10.458	187.60	6.873	1.122	8.068
Coeff. Var.	0.02	0.03	0.02	0.04	0.02	0.02

Summary statistics for major anions also reflect very narrow concentration ranges (Table 10). The chemograph for alkalinity is similar to that of Ca with a small peak three months after the peak discharge (Figure 23). The sulfate chemograph shows a small spike about one month after the peak flow followed by a decline and gradual recovery over the rest of the year (Figure 24). The chemograph of Cl is similar to that of Na (Figure 25) suggesting the influence of road salt. Fluoride and phosphate concentrations (not shown) were at or below detection limits in all samples.

Table 10: Summary statistics for concentrations of major anions.

	HCO_3 (mg/L)	Cl (mg/L)	SO_4 (mg/L)	NO_3 (mg/L)
N	65	65	65	65
Minimum	197.004	7.644	16.455	0.532
Maximum	227.112	9.656	18.794	1.197
Median	212.146	8.368	17.482	0.841
Mean	211.220	8.379	17.484	0.870
Coeff. Var.	0.03	0.06	0.03	0.17

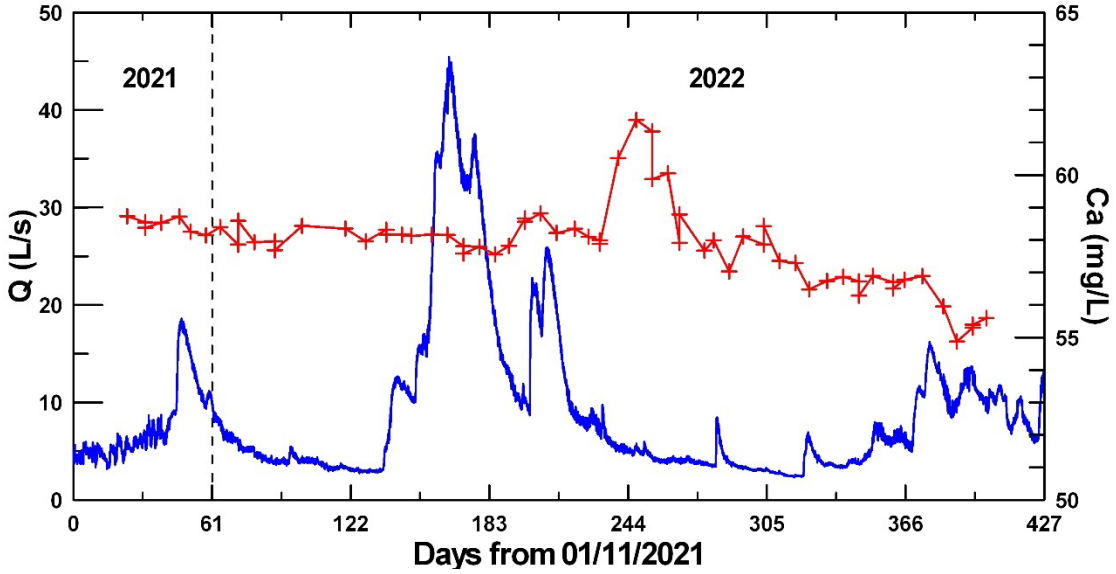

Figure 18: Chemograph of Ca concentrations (right scale) with overlay of discharge hydrograph (left scale) from November 1, 2021.

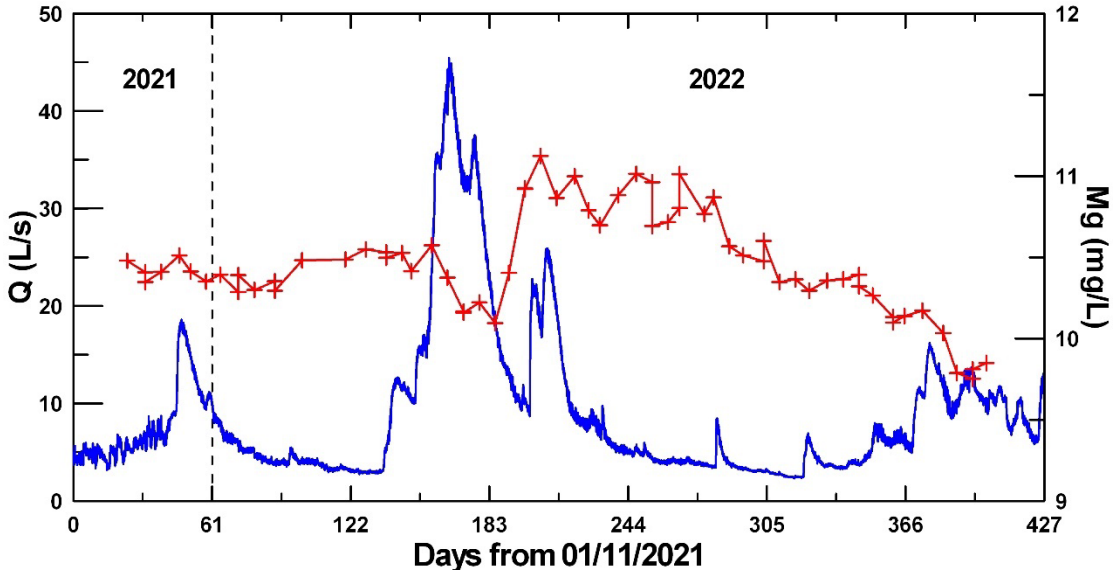

Figure 19: Chemograph of Mg concentrations (right scale) with overlay of discharge hydrograph (left scale) from November 1, 2021.

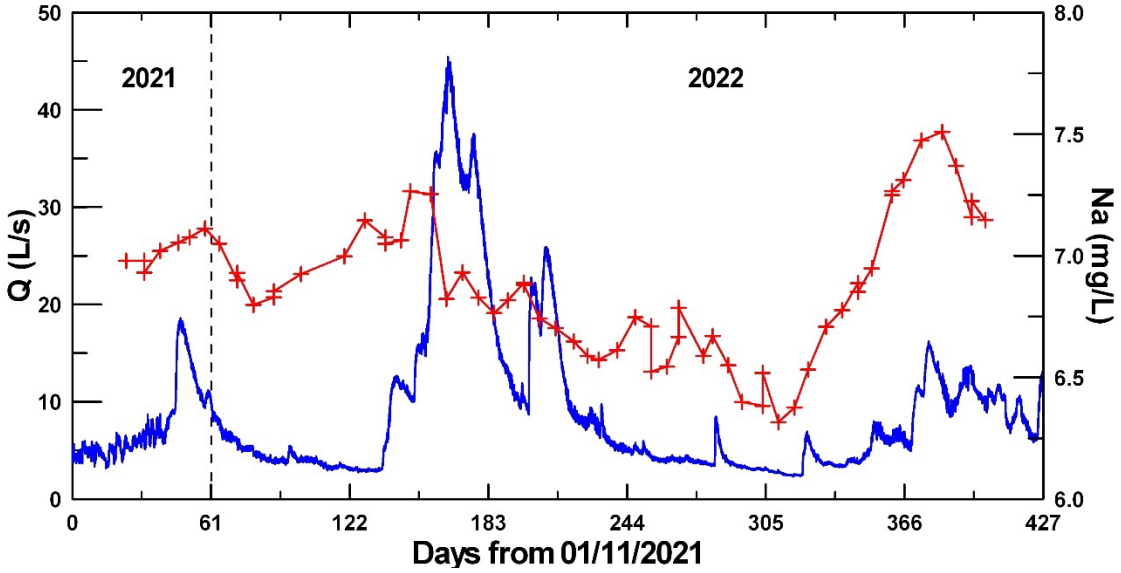

Figure 20: Chemograph of Na concentrations (right scale) with overlay of discharge hydrograph (left scale) from November 1, 2021.

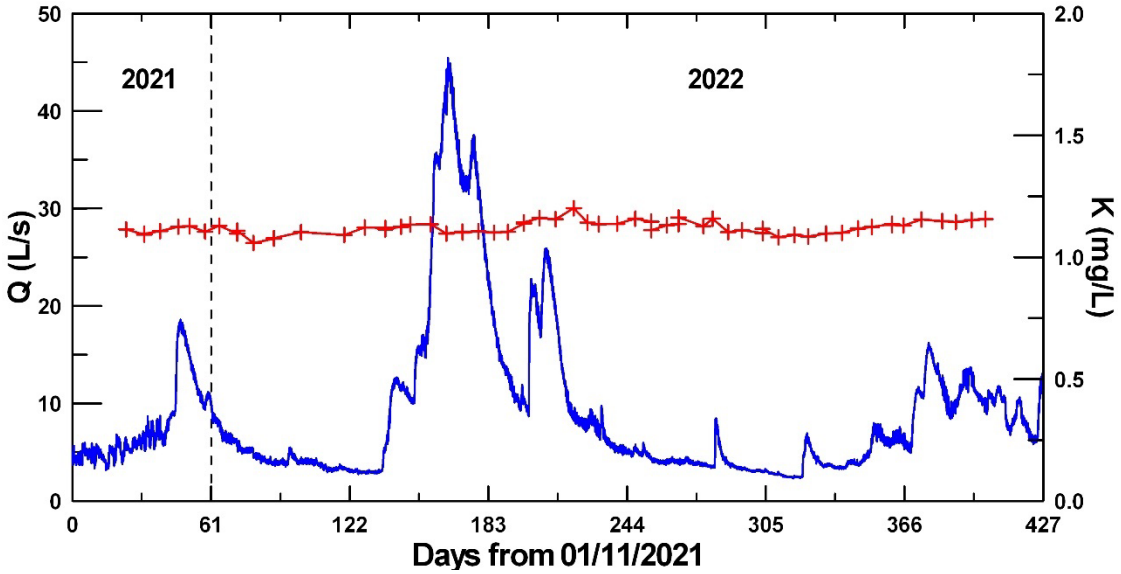

Figure 21: Chemograph of K concentrations (right scale) with overlay of discharge hydrograph (left scale) from November 1, 2021.

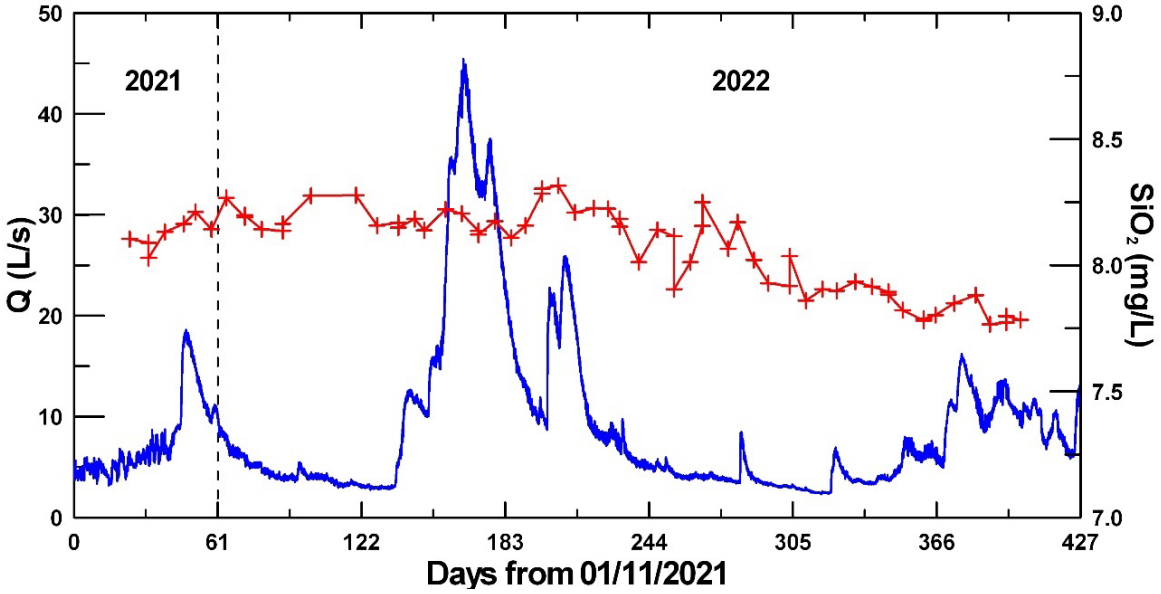

Figure 22: Chemograph of silica concentrations (right scale) with overlay of discharge hydrograph (left scale) from November 1, 2021.

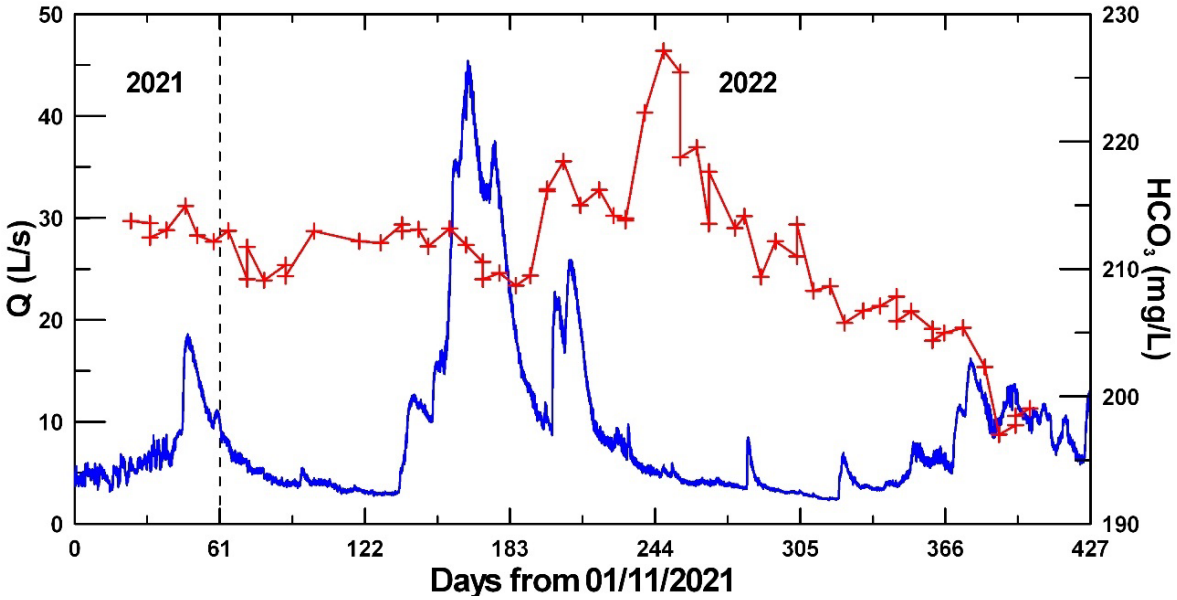

Figure 23: Chemograph of alkalinity (as bicarbonate) concentrations (right scale) with overlay of discharge hydrograph (left scale) from November 1, 2021.

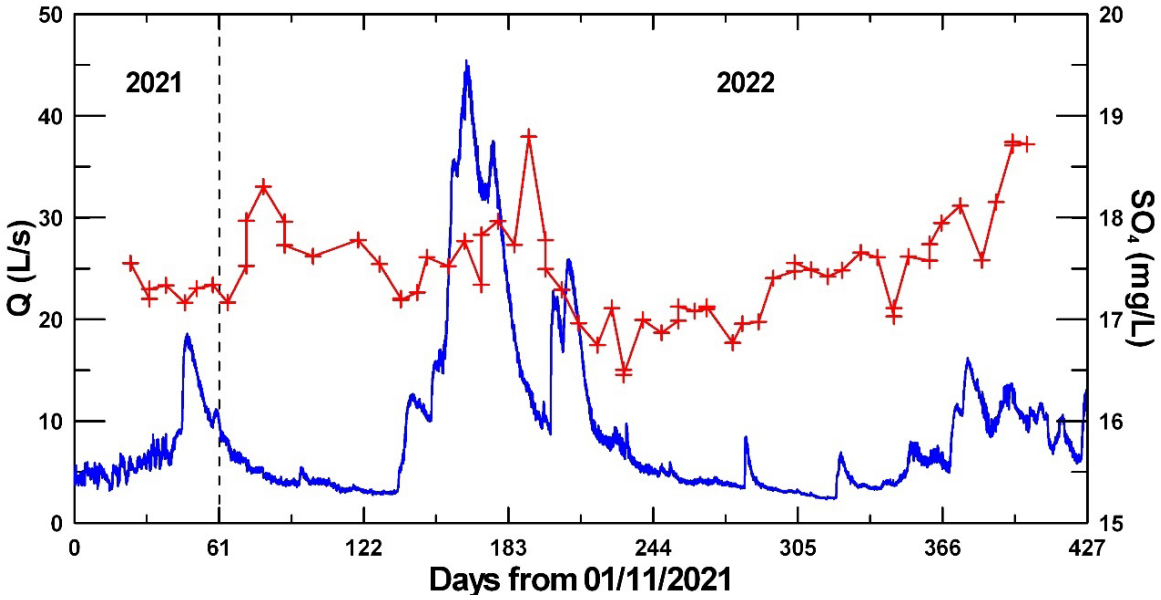

Figure 24: Chemograph of sulfate concentrations (right scale) with overlay of discharge hydrograph (left scale) from November 1, 2021.

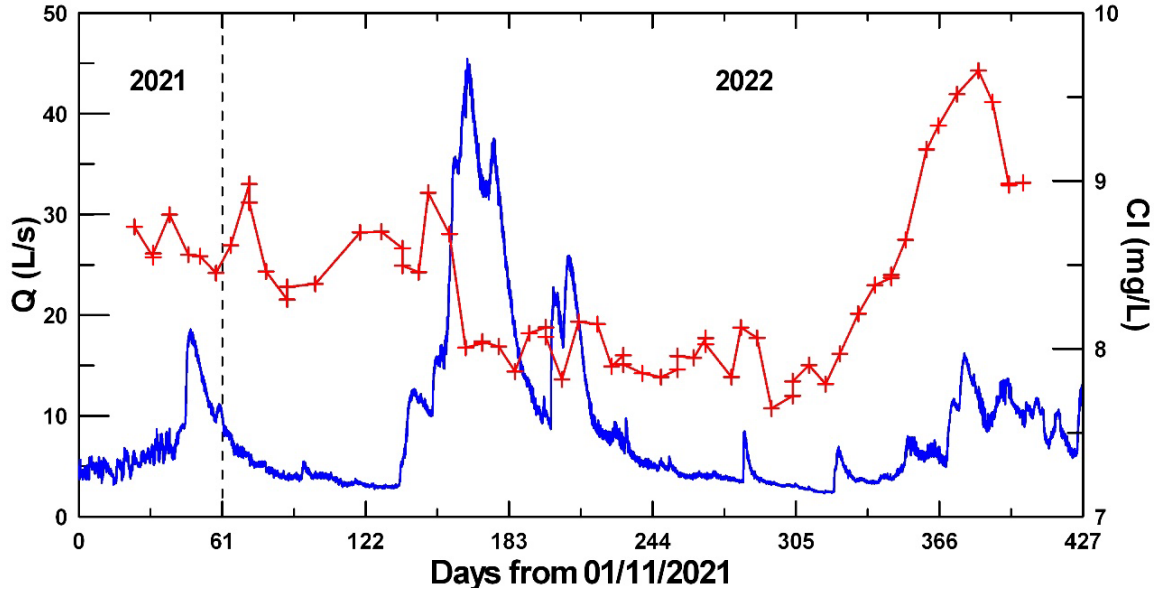

Figure 25: Chemograph of Cl concentrations (right scale) with overlay of discharge hydrograph (left scale) from November 1, 2021.

Minor Cations and Trace Elements

Summary statistics for Al and Mn concentrations in filtered (dissolved) and unfiltered (total) samples show the narrow range of variability for these cations (Table 11). Whereas about half the Al is in the suspended particulate phase (total – dissolved concentration), Mn occurs entirely in the dissolved phase. Iron concentrations are significantly higher than those of Al and Mn and exhibit much greater variability (Table 11). The chemograph of dissolved Fe is essentially flat except for a sharp spike lagging the hydrograph peak by about one and a half months (Figure 26). The chemograph of total Fe parallels that of dissolved Fe. Although particulate Fe concentrations appear relatively constant, they represent between 20.7 and 83.8 % of total Fe.

Table 11: Summary statistics for Dissolved (D) and Total (T) concentrations of minor cations.

	Al-D (µg/L)	Al-T (µg/L)	Mn-D (µg/L)	Mn-T (µg/L)	Fe-D (µg/L)	Fe-T (µg/L)
N	65	65	65	65	65	65
Minimum	1.50	2.00	12.90	12.78	16.10	67.30
Maximum	4.10	7.70	29.27	29.46	307.00	387.00
Median	1.70	2.70	16.15	16.10	29.60	118.20
Mean	1.86	2.94	17.14	17.16	55.39	130.67
Coeff. Var.	0.20	0.38	0.19	0.19	1.05	0.49

Concentrations of most trace elements of interest, except for As, exhibit little variability (Table 12). Cobalt, Ni, and Sb occur entirely in the dissolved phase. Arsenic, Cu, and Zn are mostly found in the dissolved phase whereas Ag and Pb are predominantly in the particulate phases.

Table 12: Summary statistics for Dissolved (D) and Total (T) concentrations of selected trace elements.

	Ag-D (µg/L)	Ag-T (µg/L)	As-D (µg/L)	As-T (µg/L)	Co-D (µg/L)	Co-T (µg/L)	Cu-D (µg/L)	Cu-T (µg/L)
N	65	65	65	65	65	65	65	65
Minimum	0.20	0.78	652.63	708.19	92.13	91.63	14.94	16.48
Maximum	0.51	1.48	1,021.63	1,034.65	107.25	107.71	19.01	19.82
Median	0.29	0.94	737.62	780.90	98.16	99.22	15.83	17.48
Mean	0.31	0.99	745.19	793.28	98.46	98.88	16.15	17.63
Coeff. Var.	0.23	0.17	0.10	0.09	0.04	0.04	0.05	0.05

	Ni-D (µg/L)	Ni-T (µg/L)	Pb-D (µg/L)	Pb-T (µg/L)	Sb-D (µg/L)	Sb-T (µg/L)	Zn-D (µg/L)	Zn-T (µg/L)
N	65	65	65	65	65	65	65	65
Minimum	69.12	68.85	0.10	0.50	38.71	38.43	50.01	51.90
Maximum	80.53	81.33	0.24	0.77	48.56	48.73	60.23	61.77
Median	75.84	75.74	0.14	0.64	42.12	41.99	54.22	55.25
Mean	75.91	75.89	0.15	0.64	42.23	42.19	54.32	55.35
Coef. Var.	0.03	0.03	0.20	0.10	0.05	0.05	0.04	0.04

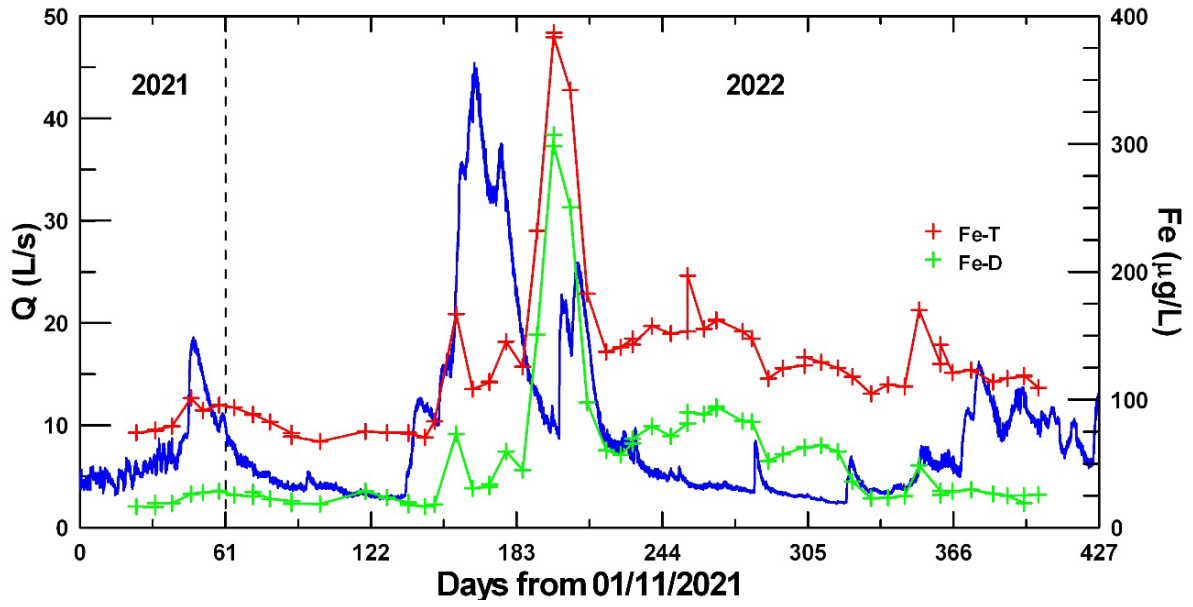

Figure 26: Chemograph of dissolved (D) and total (T) Fe concentrations (right scale) with overlay of discharge hydrograph (left scale) from November 1, 2021.

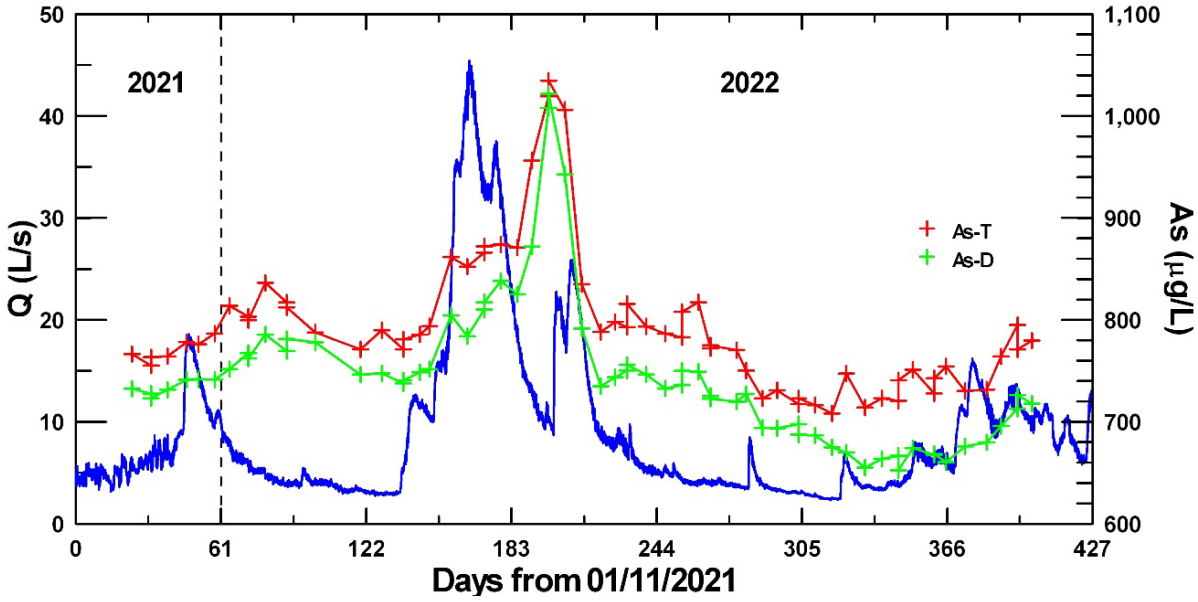

Figure 27: Chemograph of dissolved (D) and total (T) As concentrations (right scale) with overlay of discharge hydrograph (left scale) from November 1, 2021.

The chemograph of dissolved As is relatively featureless except for a pronounced spike approximately one month after peak freshet flow (Figure 27). The chemograph of total As follows the same pattern. Arsenic in the particulate phase does not exhibit any clear temporal trend (not shown) and it represents between 1.1 and 12.5 % of the total As concentration in mine water.

Temporal variations in Co concentrations are subtle in terms of their magnitude but exhibit features that are related to the discharge hydrograph (Figure 28). In particular, the peak Co concentration closely follows the peak freshet and lowest concentrations are observed during early fall low-flow conditions.

Temporal variations in Ni concentrations appear almost antithetical to those of Co (Figure 29). The lowest Ni concentrations are observed about one month following peak freshet flow whereas the highest values occur during fall low-flow conditions.

The chemograph for Sb shows minor peaks lagging hydrograph peaks by about one month (Figure 30). Antimony concentrations trend upwards during the fall months to reach a maximum in late November of 2022.

The Zn chemograph exhibits a spike that lags peak discharge by less than two weeks. Otherwise, variations in Zn concentrations are a subdued reflection of discharge flow rates (Figure 31).

The chemographs for Cu (Figure 32) and Ag (Figure 33) follow a similar pattern to that of Zn. Indeed, the concentrations of Zn, Cu, and Ag are strongly correlated (not shown).

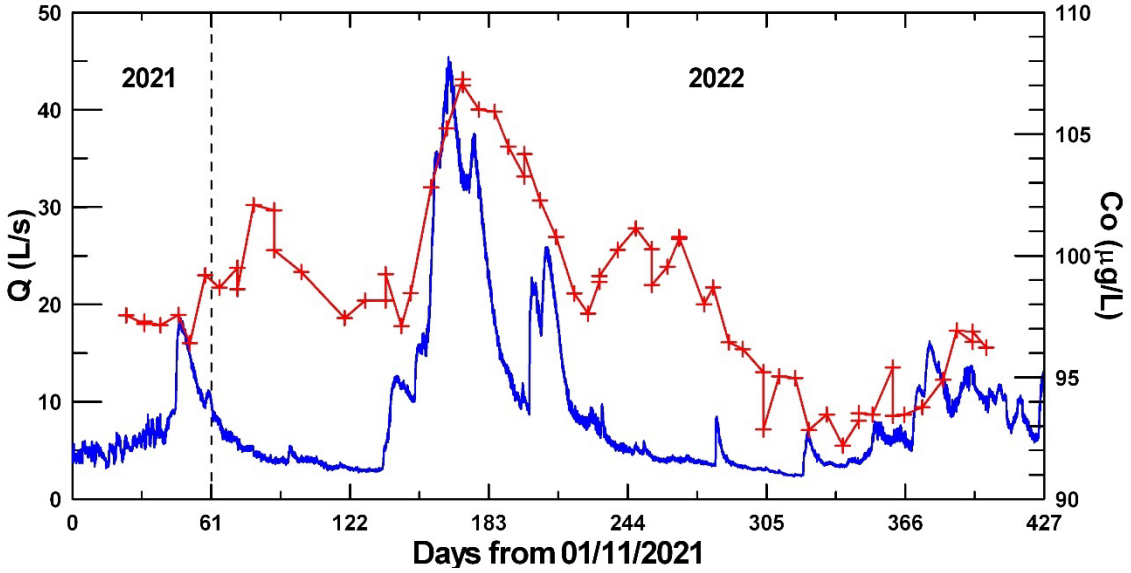

Figure 28: Chemograph of Co concentrations (right scale) with overlay of discharge hydrograph (left scale) from November 1, 2021.

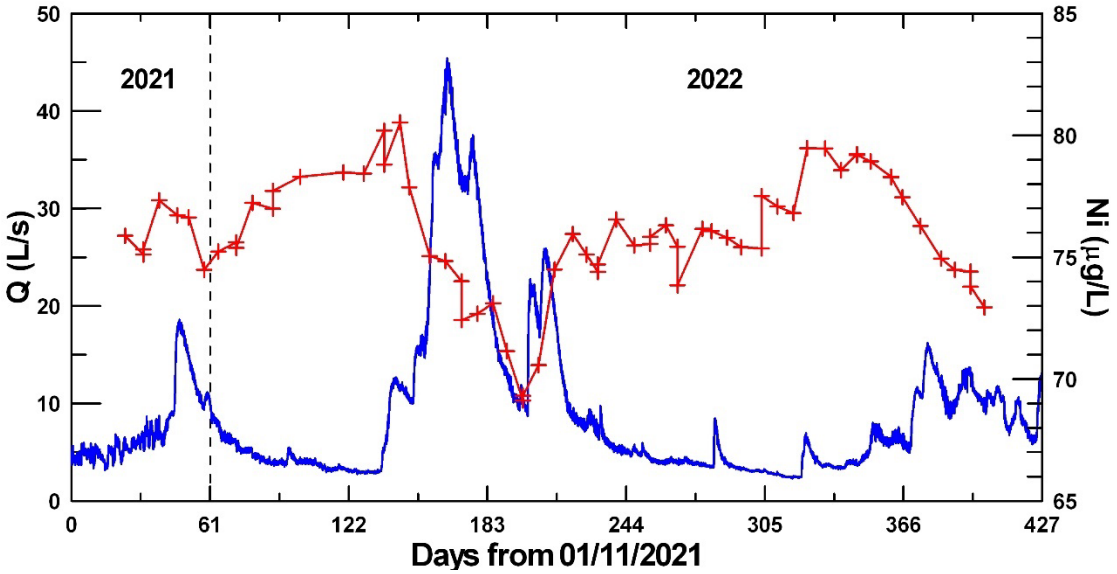

Figure 29: Chemograph of Ni concentrations (right scale) with overlay of discharge hydrograph (left scale) from November 1, 2021.

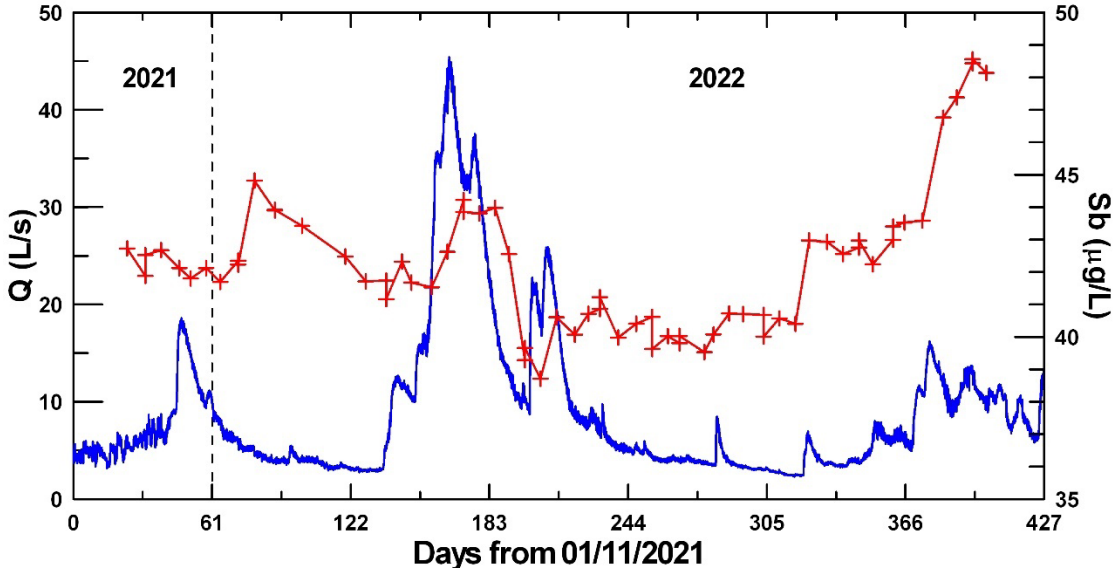

Figure 30: Chemograph of Sb concentrations (right scale) with overlay of discharge hydrograph (left scale) from November 1, 2021.

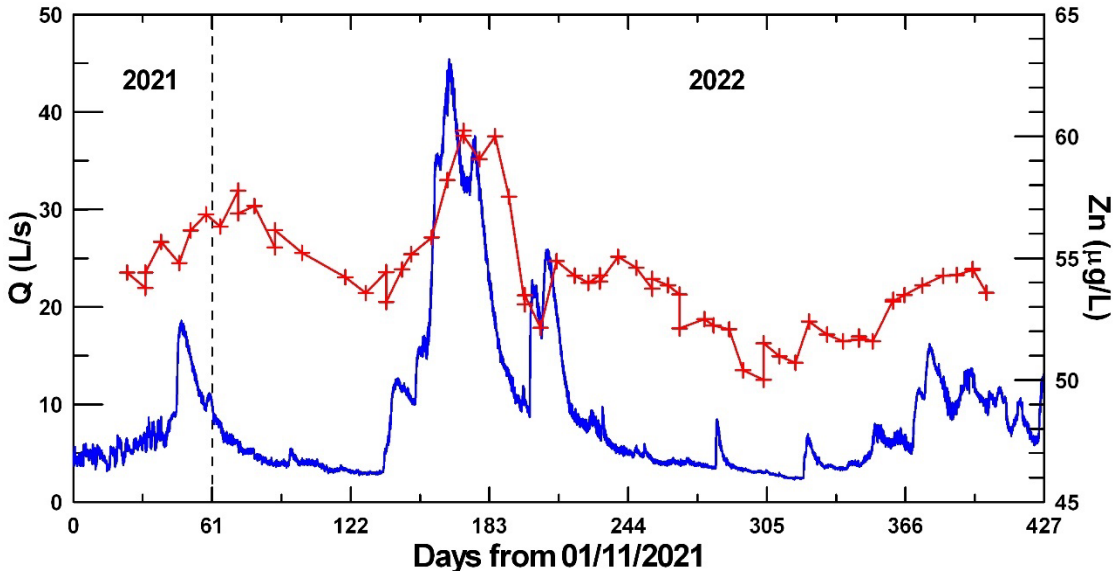

Figure 31: Chemograph of Zn concentrations (right scale) with overlay of discharge hydrograph (left scale) from November 1, 2021.

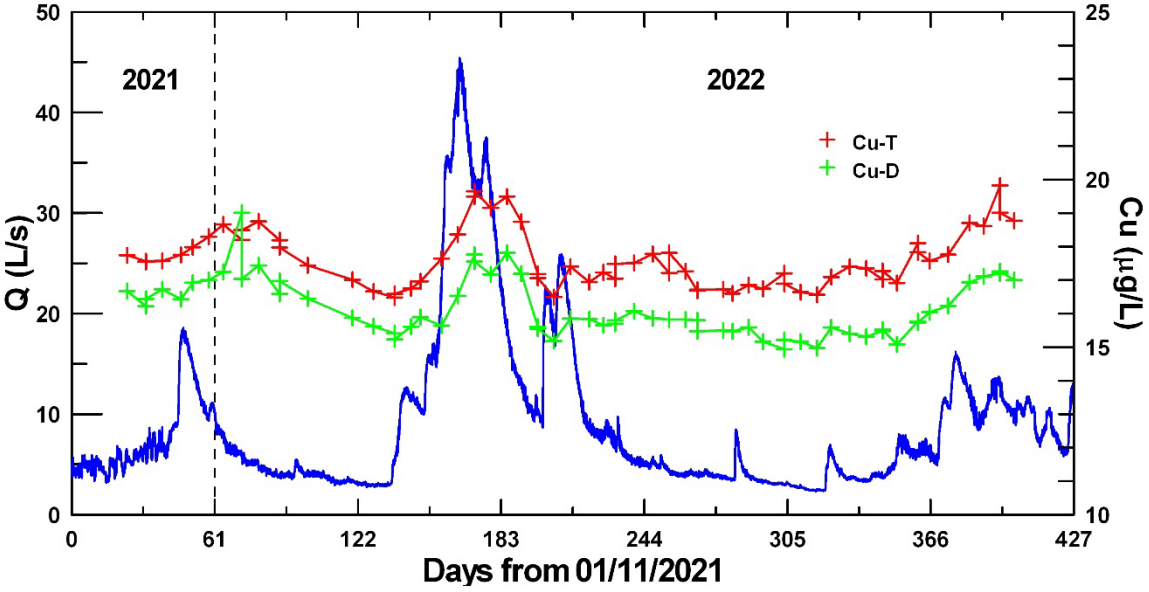

Figure 32: Chemograph of Cu (Total and Dissolved) concentrations (right scale) with overlay of discharge hydrograph (left scale) from November 1, 2021.

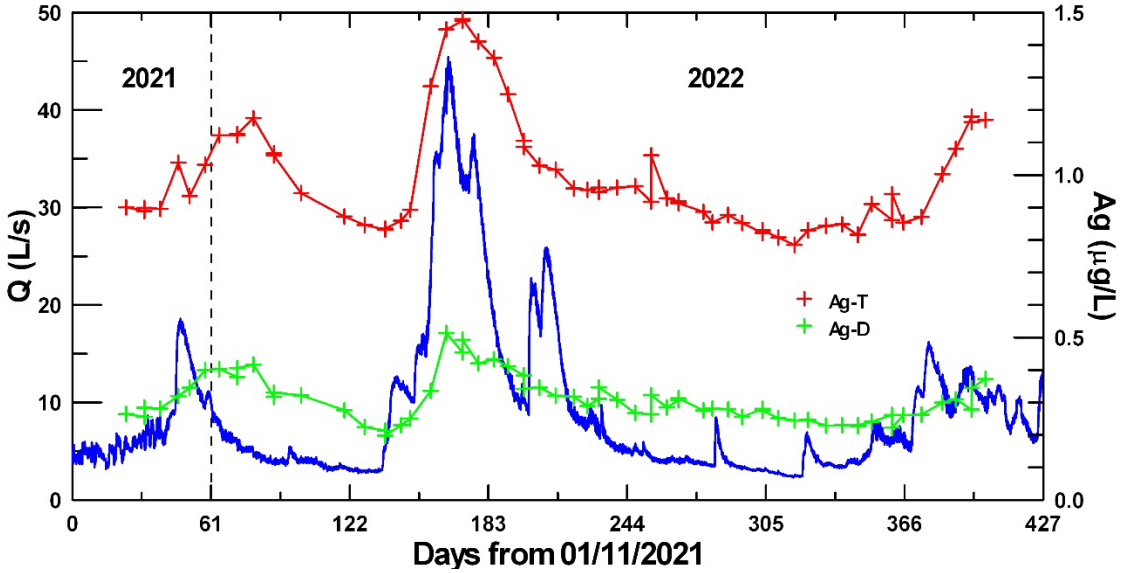

Figure 33: Chemograph of Ag (Total and Dissolved) concentrations (right scale) with overlay of discharge hydrograph (left scale) from November 1, 2021.

5.0 DISCUSSION

5.1 Conceptual hydrogeological model

Excavation of the Nipissing and adjacent mines, and their subsequent flooding, has created an anthropogenic, topographically driven, groundwater flow system. All meteoric recharge and water bodies falling within its capture zone ultimately discharge at Shaft 98. The boundaries of the capture zone are defined by groundwater flow lines shaped by the terrain and the complex network of connected mine workings.

Most recharge to the groundwater flow system is likely to occur on the hill west of Shaft 98, on the sites of the former Coniagas and Trethewey mines. Focalized recharge to mine workings will occur directly through large open cuts on the surface of these properties. Lesser recharge will be in the form of distributed fracture-controlled infiltration. Given the elevations of Sasaginaga Lake (circa 306 m) and Cobalt Lake (circa 292 m) relative to the collar elevation of Shaft 98 (284 m), recharge from these lakes is also possible. However, water stable isotope data do not show any sign of evaporative enrichment suggesting that any recharge from lakes is likely minor.

In 2022, the total mine water discharge from Shaft 98 was 289,541 m^3. Based on the full two-year flow monitoring period, the average annualized discharge was 278,529 m^3. This volume is equivalent to a 65 m cube. Based on data from the Ville Marie and Earlton weather stations (Tables 1 and 2), average annual precipitation in the Cobalt area is estimated at 811 mm. Assuming 100 % infiltration of precipitation (no runoff), no significant evapotranspiration, and no recharge from lakes, the minimum capture zone area for the Shaft 98 groundwater flow system would be approximately 343,440 m^2, which is equivalent to a recharge area 586 m square.

Figure A-1 (Appendix 1) shows a longitudinal section of mine workings along the Meyer vein where the collar elevation of the No. 73 (Meyer) Shaft is 299 m (982 ft). Given that Shaft 73 does not flow, the water level in the mine pool should not exceed that elevation. This implies that open stopes on the western edge of the Nipissing property and on the Coniagas and Trethewey properties will be partially or totally within the unsaturated zone. Therefore, exposed sulphide and sulpharsenide minerals on the walls of the workings are susceptible to oxidation and will form more soluble secondary minerals. Because the workings are inaccessible, confirmation of these minerals is not possible, but they may include scorodite, pharmacolite, erythrite, and annabergite. Moisture on the walls will equilibrate with these minerals and solutes will be flushed periodically by infiltrating waters. Metal(loid)-laden leachate will report to the mine pool where it will mix with older water on the way to the discharge point at Shaft 98. The mean residence time of this impacted recharge depends on the flow rate through the groundwater system (circa 280,000 m^3/yr.) relative to the volume of the mine pool. While the volume of the mine pool is unknown, some mine workings connected to Shaft 98 extend almost down to sea level (Shaft 64) although the rest are above an elevation of 132 m (434 ft) as shown in Figure A-2 (Appendix 1). Therefore, the volume of the mine pool is most probably very large compared to annual discharge. Mine water residence times in the Shaft 98 capture zone are likely to be correspondingly long. The very low temporal variability of most hydrochemical parameters observed in drainage is evidence of long residence times and thorough groundwater mixing in the mine pool.

5.2 Sorption and redox controls on arsenic concentrations

Arsenic in mine water discharge is likely derived from the dissolution of secondary arsenate minerals such as scorodite, erythrite, and pharmacolite, themselves formed by the oxidation of primary arsenide and sulpharsenide minerals (Table 4). In oxic groundwaters and at circumneutral pH, As preferentially sorbs on to suspended particulate hydrous ferric oxides (HFO), if present. In drainage from Shaft 98, particulate Fe accounts for between 20.7 and 83.4 % of total Fe while particulate As varies between 1.1 and 12.5 % of total As (Table 14). The weak correlation between particulate As and Fe concentrations (Figure 34a) suggests that some As is sorbed on particulate Fe. The As/Fe molar ratio (total concentrations) varies from 1.9 to 8.7, with a median value of 4.8. This indicates that mine water chemistry is Fe-limited and sorption of As on HFO does not appear to be a major control on As concentrations. However, the strong correlation between dissolved As and Fe concentrations (Figure 34b) suggests other controlling processes.

Table 13: Summary statistics for suspended particulate (> 0.45 µm) concentrations of Fe and As and their percentages of total Fe and As concentrations, respectively.

	Particulate Fe (µg/L)	Particulate Fe (%)	Particulate As (µg/L)	Particulate As (%)
N	65	65	65	65
Minimum	48.8	20.7	9.8	1.1
Maximum	121.6	83.4	94.0	12.5
Median	75.1	70.2	46.9	5.9
Mean	75.3	63.5	48.1	6.1
Coef. Var.	0.21	0.24	0.38	0.38

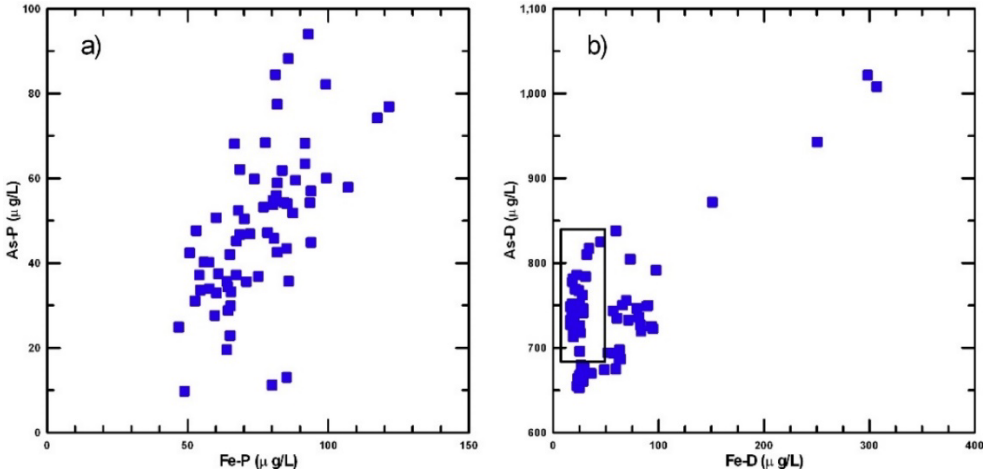

Figure 34: Concentration of As versus concentration of Fe: particulate (a); dissolved (b). Box in (b) encompasses data from the fall and winter of 2021-2022 when Fe values were almost constant. Outlier data points in (b) are associated with low ORP values.

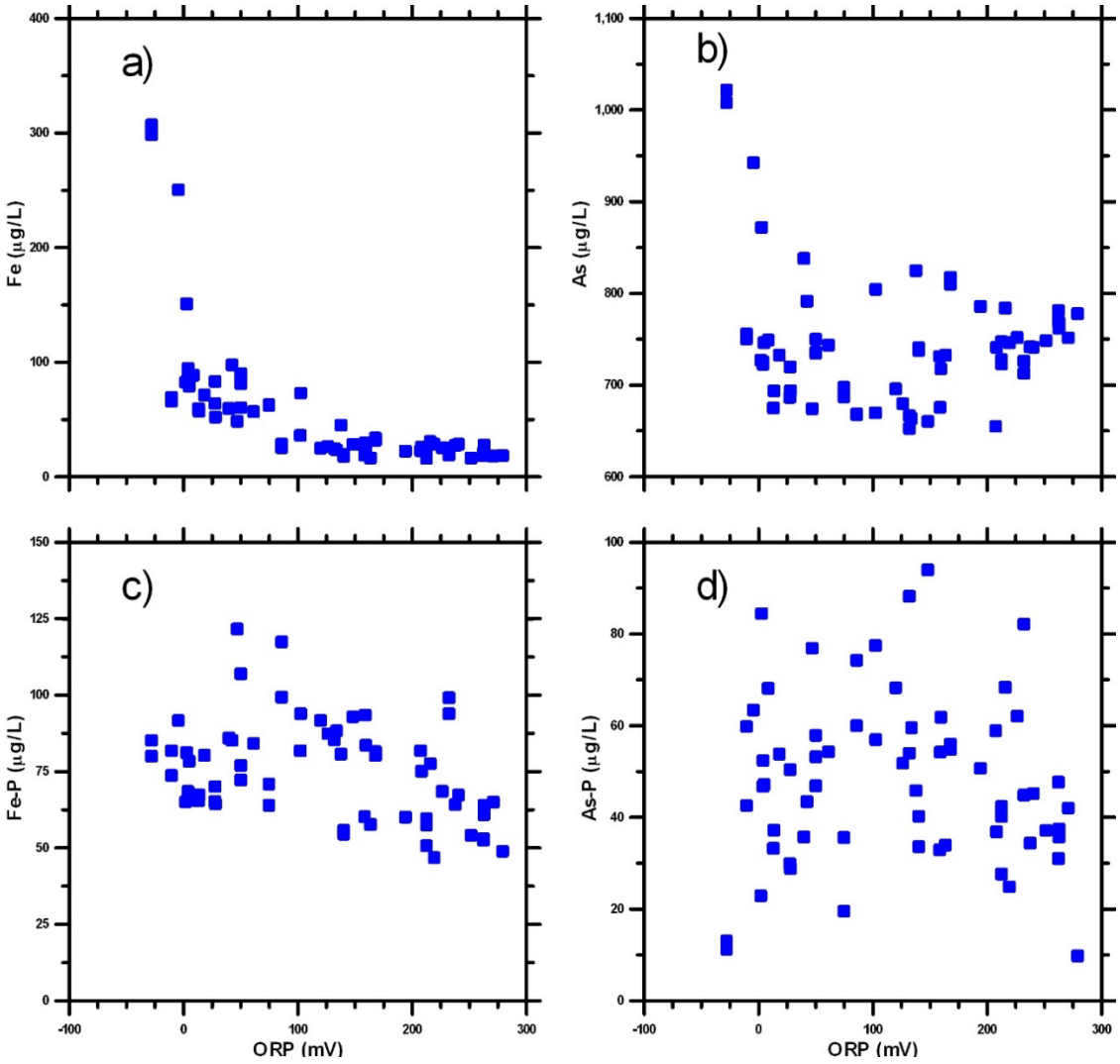

Figure 35: Fe (dissolved) concentration versus ORP (a); As (dissolved) concentration versus ORP (b); Fe (particulate) concentration versus ORP (c); As (particulate) concentration versus ORP (d).

Under reducing conditions, reductive dissolution of HFO releases any sorbed As and leads to higher dissolved ferrous Fe and As concentrations. Here, Fe concentrations increase sharply as ORP decreases below 50 mV (Figure 35a). Arsenic concentrations follow a similar pattern (Figure 35b). On the other hand, ORP does not seem to have any effect on particulate concentrations of Fe and As (Figure 35c, d). It is also apparent that dissolution of particulate Fe and As concentrations could not account for the high Fe and As values observed at low ORP. It would seem that the spike in Fe and As following the freshet (Figures 26, 27) reflects the passage of a slug of old, reducing water from a distinct source in the deep mine pool rather than reductive dissolution of HFO in normal discharge. Because the duration of this study was limited to one year, it is unclear if the spike in reducing mine water is an annual event following the freshet. However, the absence of Fe staining in the flume in 2021 suggests that slugs of reducing mine water may be episodic.

5.3 Controls on cobalt and nickel concentrations

Cobalt and nickel in mine drainage are likely derived mainly from the dissolution of erythrite and possibly annabergite. These secondary arsenate minerals are formed by the oxidation of primary Co and Ni arsenides and sulpharsenides (Table 4). Based on the stoichiometry of these arsenates, dissolved concentrations of Co and Ni should be correlated with those of As. If high-As data from the low-ORP mine water source are discounted, this is indeed the case for Co (Figure 36a). However, the relationship between Ni and As is less clear (Figure 36b). For this reason, it is likely that Ni is mainly derived from erythrite, where it can substitute for Co (Clarke, 2017).

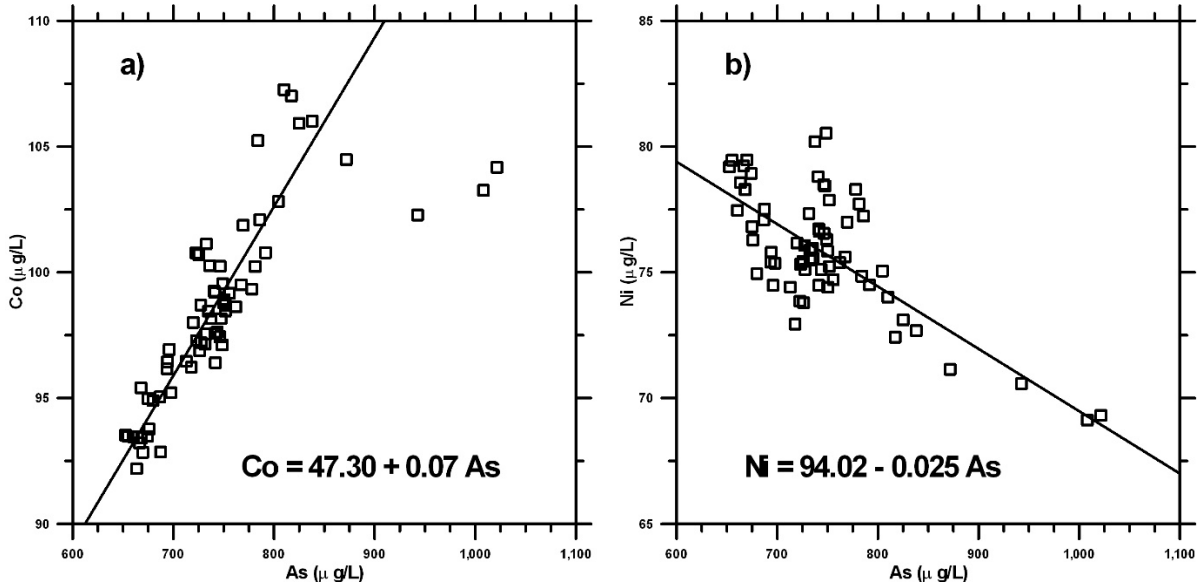

Figure 36: Concentrations of Co (a) and Ni (b) versus concentration of As. The lines and their equations represent linear least-square regressions with bi-square weighting to minimize effect of outlier data points. Outlier high-As data are associated with low ORP values.

Geochemical modeling of erythrite dissolution by SRK (2016) suggested that solubility limits for As and Co were 16 mg/L and 1.9 mg/L, respectively. The expected As/Co weight ratio would then be 8.4. A histogram of Co/As molar ratios computed on mine drainage samples indicates a range of values (Figure 37a). The observed median molar Co/As value of 0.17 corresponds to a median As/Co ratio of 5.88 or to a weight ratio of 7.48. Given that not all As is in the dissolved phase, this value is fairly close to the SRK estimate. The histogram of Ni/As molar ratios shows a range of values with a median of 0.13 (Figure 37b). This value corresponds to a median As/Ni molar ratio of 7.69 or a weight ratio of 9.82.

Dissolved Co concentrations tend to decrease with increasing pH (Figure 38a). A similar relationship is found for As (not shown) when the low-ORP data are disregarded. Concentrations of Ni appear unaffected by variations in pH (Figure 38b). Concentrations of Co and Ni do not exhibit any correlation with ORP (not shown).

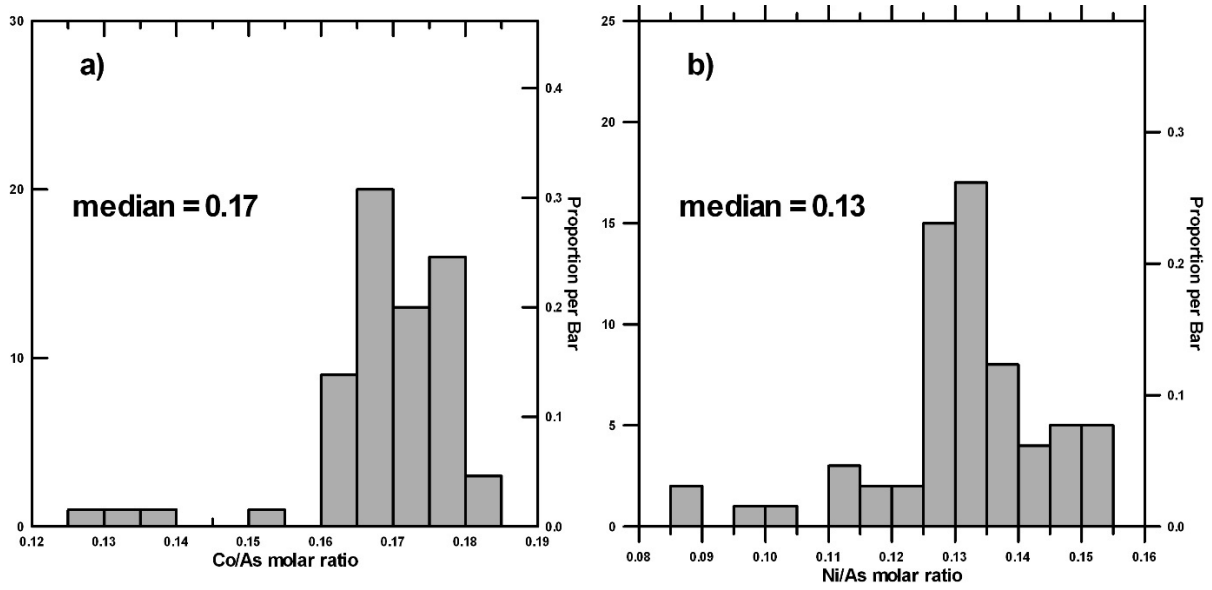

Figure 37: Histograms of Co/As (a) and Ni/As (b) molar ratios for dissolved constituents.

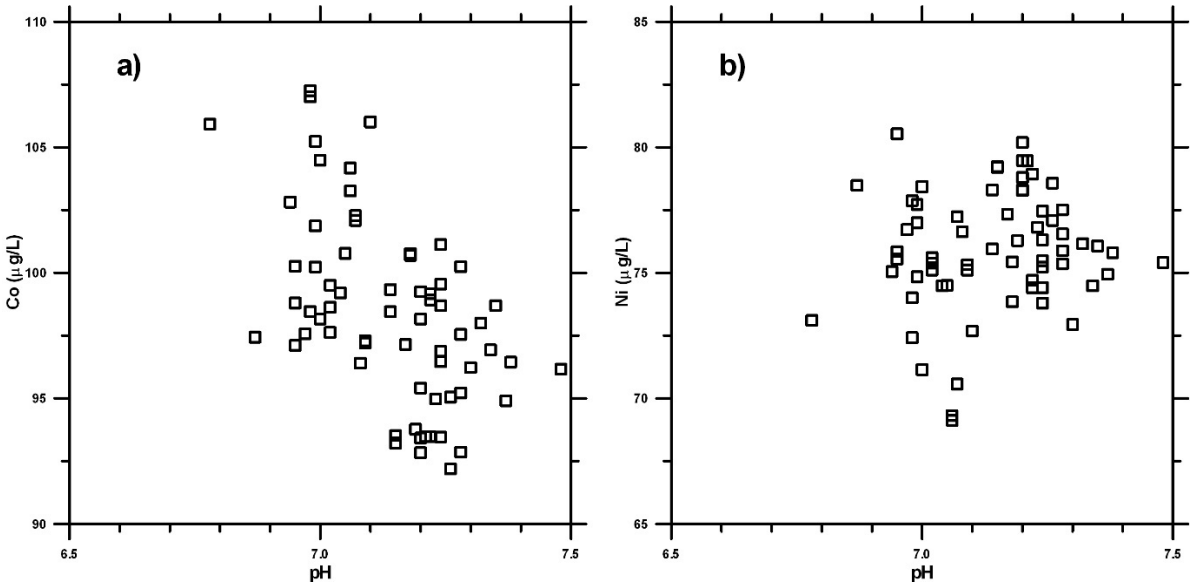

Figure 38: Cross-plots of dissolved Co (a) and Ni (b) versus pH.

5.4 Concentration-Discharge relationships

In catchment hydrology, relationships between the discharge rate of a stream or river and the concentrations of its solutes are used to infer biogeochemical weathering processes within its watershed and exported solute loads (Brooks et al., 2015). Observations have shown that power-law relationships between solute concentration (C) and discharge (Q) are ubiquitous (Hall, 1970; 1971; Wymore et al., 2023). Although more sophisticated C-Q models have been proposed (Godsey et al., 2009; Thompson et al., 2011; Maher and Chamberlain, 2014), they are beyond the scope of this report. Here, this hydrological approach is applied to a preliminary analysis of the export of solutes from the Shaft 98 "catchment".

A C-Q power-law model ($C = \alpha Q^{\beta}$) is characterized by its parameters, α and β. It can be derived from first principles assuming a power-law relation between storage volume and discharge, ideal mixing, and a constant mass solute source (Hall, 1970). On log-log scales, the model plots as a straight line with intercept α and slope β. The value of β is used to characterize the weathering behaviour of a solute. A slope close to zero is indicative of "chemostatic" behaviour where solute concentrations are independent of flow rates. Non-zero positive or negative slopes indicate "chemodynamic" behaviour. A positive slope is interpreted to represent solute flushing whereas a negative slope suggests dilution. A slope of -1 indicates pure dilution.

Another metric for characterizing C-Q relationships is the ratio of their respective coefficients of variations (Thompson et al., 2011). This dimensionless metric (CV_C / CV_Q) compares the variability of solute concentrations to the variability of discharge rates. In conjunction with β, it distinguishes concentration variability due to a relationship with Q from variability due to other factors.

To display concentration-discharge (C-Q) relationships for solutes in Shaft 98 drainage, discharge rates and concentrations are normalized relative to values hypothesized to represent baseflow conditions. Discharge rates are normalized by the minimum observed flow during water chemistry sampling (2.462 L/s), which occurred on September 14, 2022. Solute concentrations are normalized by their values observed on the same date (Table 14). Field parameter and $\delta^{18}O$ values are not normalized. Plots of field parameters and $\delta^{18}O$ versus discharge are shown in Figure 39 along with fitted power models. Plots of normalized concentrations versus normalized discharge are shown in Figures 40, 41, and 42. These plots also show the non-linear least-squares power-law model fitted to the data. Non-linear regression using Gauss-Newton iteration was performed using SYSTAT ®. The normalization of C and Q affects the power-law intercept α but not the slope β.

Metrics (CV_C / CV_Q and β) for the field parameters, $\delta^{18}O$, cations, anions, and trace elements are summarized in Table 15 along with confidence intervals on β and regression R^2. Using CV_C / CV_Q and β criteria, Musolff et al. (2015) proposed definitions for chemostatic ($-0.2 < \beta < 0.2$ and $CV_C/CV_Q < 0.5$) and chemodynamic ($\beta < -0.2$ or $\beta > 0.2$ and $CV_C/CV_Q > 0.5$) solute behaviour. According to these criteria, all the parameters listed in Table 15 are classified as chemostatic, with the exception of DO and ORP. However, closer inspection of individual C-Q plots reveals more subtle flushing and dilution trends.

Table 14: Drainage concentrations observed on September 14, 2022, as used to normalize solute data. Discharge rates are normalized by the corresponding flow rate (2.462 L/s) on the same date.

	Ca (mg/L)	Mg (mg/L)	Na (mg/L)	K (mg/L)
Normalizing value	57.29	10.37	6.38	1.10

	SiO_2 (mg/L)	NO_3 (mg/L)	SO_4 (mg/L)	Cl (mg/L)
Normalizing value	7.90	0.91	17.42	7.79

	As (µg/L)	Co (µg/L)	Ni (µg/L)	Sb (µg/L)
Normalizing value	674.98	94.97	76.81	40.40

Drainage proton (H) activity (for pH) exhibits a slight relationship with Q (Figure 39a), with a significant value for β (0.187) but low R^2 (Table 15). The relationship between DO and Q shows a well-defined power-law behaviour with a β value of -0.318 and an R^2 value of 0.614 (Figure 39b). The C-Q plot for ORP does not suggest any relationship with Q (Figure 39c). Indeed, the CV_C/CV_Q metric for ORP (0.9) suggests that factors other than Q are responsible for its variability. Similarly, the C-Q power-law model fit to $\delta^{18}O$ is poor (Figure 39d) with β not statistically different from 0 and a low R^2 value (Table 15). The main reason for the poor fit is that $\delta^{18}O$ data exhibit two distinct trends. With increasing freshet flows, there is a trend of isotopic enrichment with higher Q. With increasing Q in the fall months, $\delta^{18}O$ values become more depleted. Taken together, these results suggest that freshet discharge consists of mine water with lower pH (higher H) and DO, and $\delta^{18}O$ closer to its annual average.

The C-Q behaviour of Ca and Mg is clearly chemostatic (Figure 40a,b), with low CV_C/CV_Q values and β values not statistically different from 0 (Table 15). Sodium concentrations exhibit a slight relationship with Q (Figure 40c), with a β of 0.024 and R^2 of 0.17 (Table 15). However, as with $\delta^{18}O$, Na exhibits distinct flushing trends associated with freshet and autumn flows, respectively. For K, the power-law model fit yields a β value not statistically different from 0 (Table 15) although a plot of the data suggests a behaviour similar to that of Na (Figure 40d).

Table 15: Ratios of the coefficients of variation of solute concentrations and discharge based on Tables 9, 10, and 12. For discharge rates (Q) measured on the water sampling dates, the coefficient of variation (CV_Q) is 0.867; Power-law exponents (β) fitted to the C-Q models; Wald 95 % confidence interval on β; R^2 (Observed vs Predicted) for non-linear regression. Shaded cells indicate β values not statistically different from 0.

	H	DO	ORP	$\delta^{18}O$
CV_C/CV_Q	0.023	0.289	0.900	0.008
β	0.187	-0.318	0.152	-0.001
Wald 95 % C.I.	0.084 / 0.291	-0.385 / -0.250	-0.115 / 0.418	-0.004 / 0.001
R^2 (Obs. vs Pre.)	0.158	0.614	0.020	0.020

	Ca	Mg	Na	K
CV_C/CV_Q	0.025	0.034	0.046	0.027
β	-0.003	-0.010	0.024	0.007
Wald 95 % C.I.	-0.011 / 0.005	-0.020 / 0.001	0.010 / 0.037	-0.001 / 0.016
R^2 (Obs. vs Pre.)	0.010	0.050	0.170	0.048

	SiO_2	NO_3	SO_4	Cl
CV_C/CV_Q	0.023	0.191	0.033	0.067
β	0.006	-0.039	0.011	0.013
Wald 95 % C.I.	-0.001 / 0.014	-0.101 / 0.022	0.001 / 0.021	-0.008 / 0.034
R^2 (Obs. vs Pre.)	0.050	0.027	0.069	0.024

	As	Co	Ni	Sb
CV_C/CV_Q	0.112	0.043	0.037	0.059
β	0.067	0.031	-0.024	0.024
Wald 95 % C.I.	0.036 / 0.097	0.020 / 0.042	-0.034 / -0.014	0.006 / 0.042
R^2 (Obs. vs Pre.)	0.228	0.319	0.261	0.101

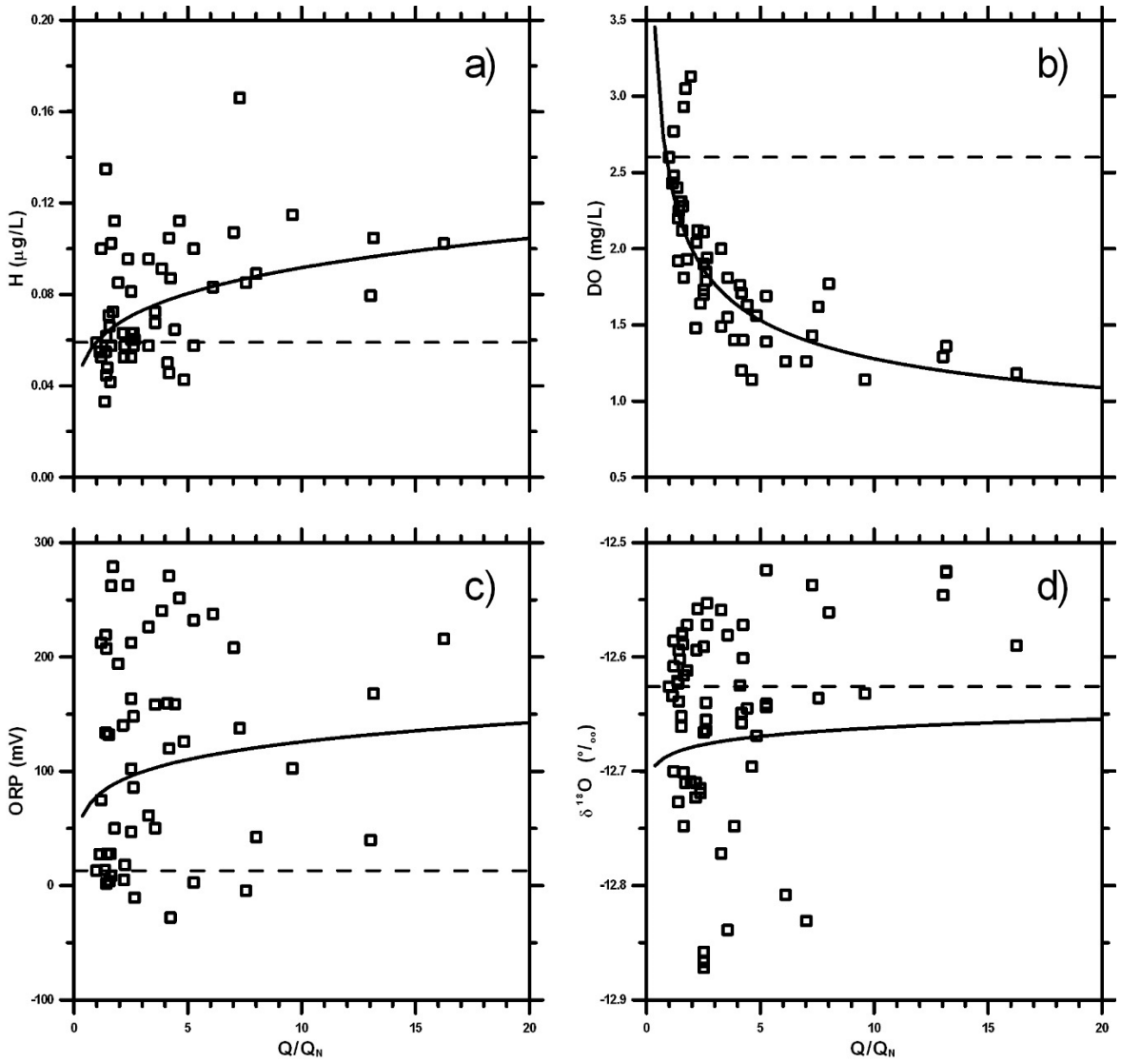

Figure 39: Concentration-Discharge (C-Q) relationships and power-law models for $H=10^{-pH}$ (a); DO (b); ORP (c); and $\delta^{18}O$ (d). Dashed lines mark parameter values observed on September 14, 2023; H (0.059) or pH (7.23); DO (2.6 mg/L); ORP (13 mV); $\delta^{18}O$ (-12.63 ‰).

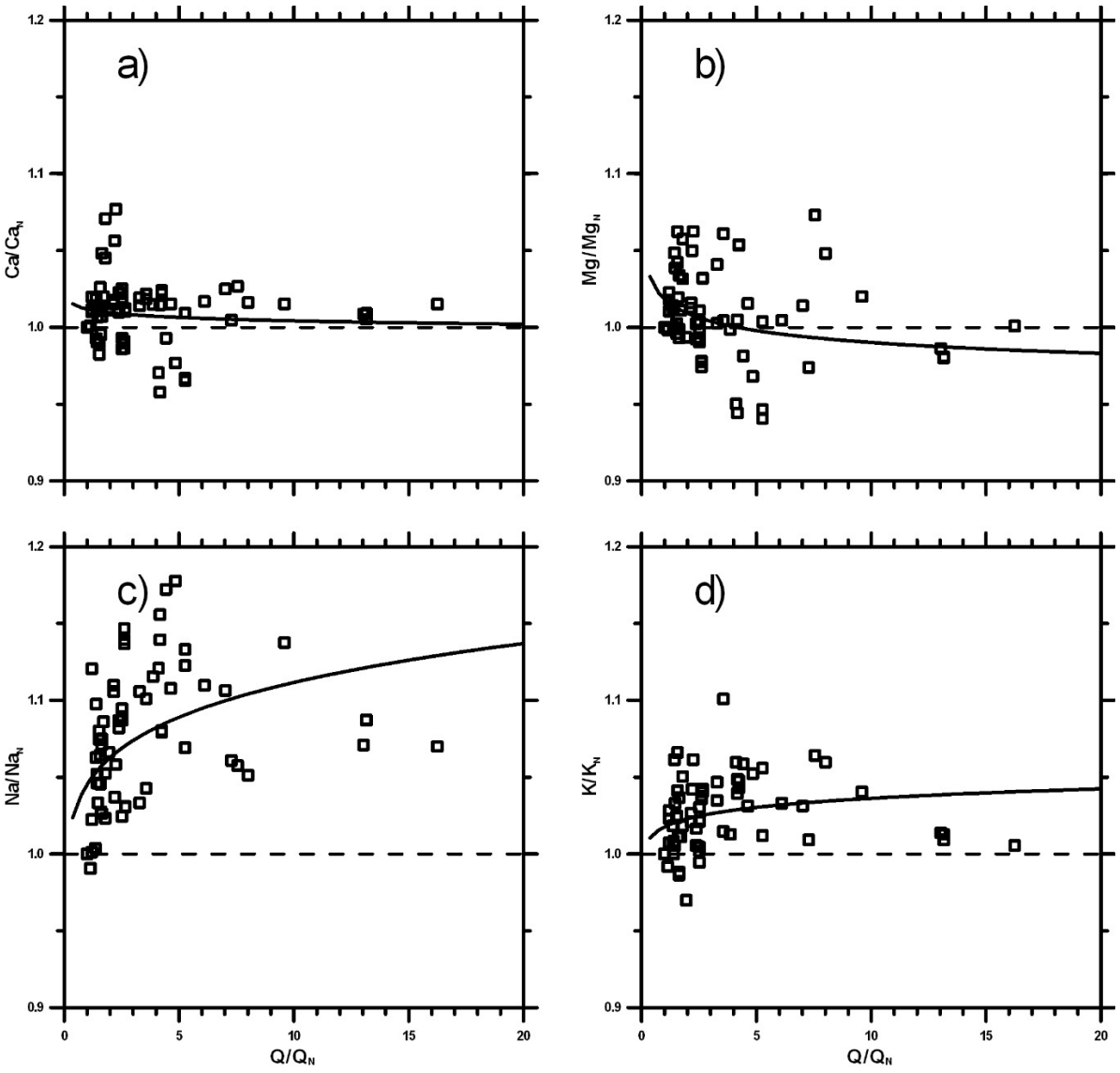

Figure 40: Concentration-Discharge (C-Q) relationships and fitted power-law models for Ca (a); Mg (b); Na (c); and K (d).

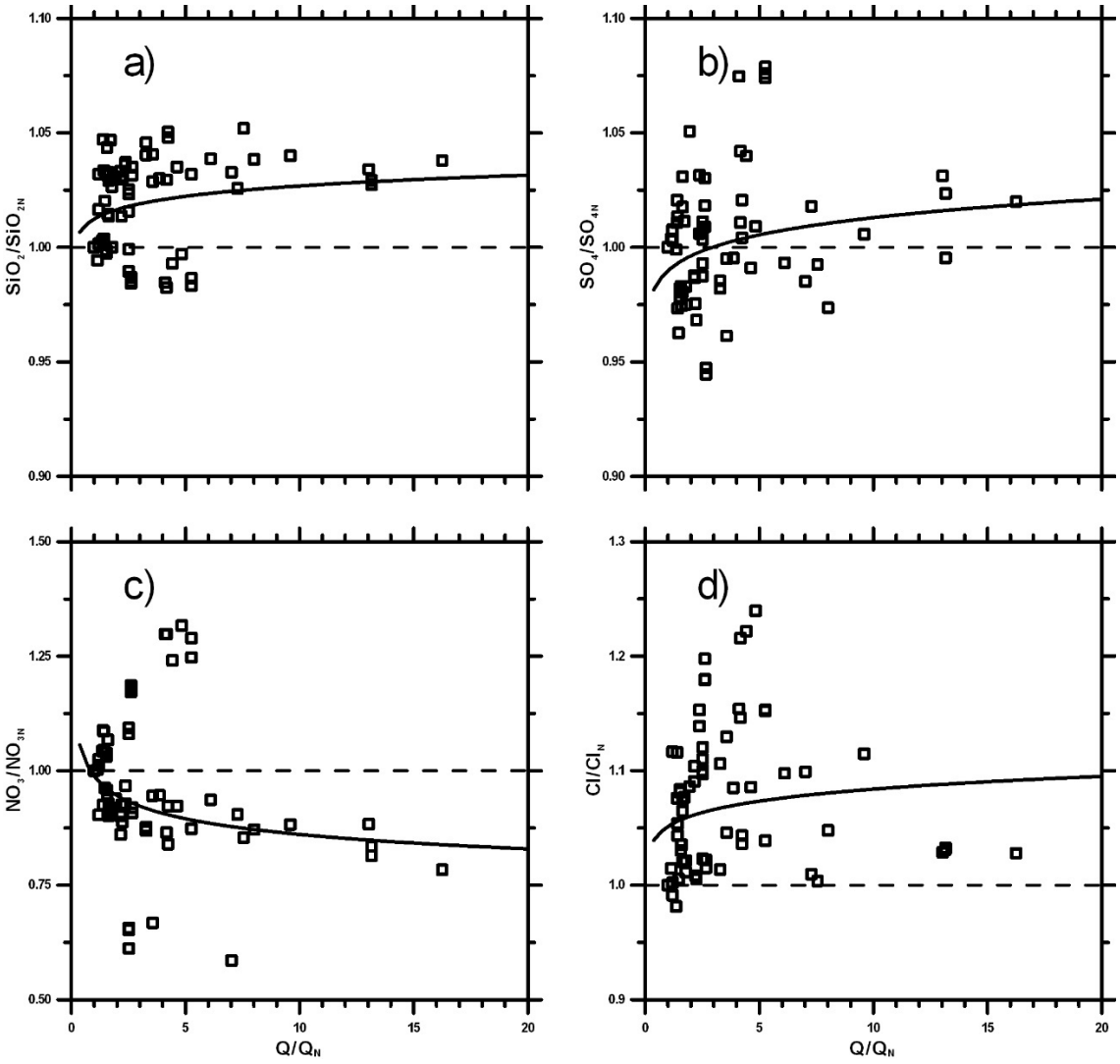

Figure 41: Concentration-Discharge (C-Q) relationships and fitted power-law models for SiO_2 (a); SO_4 (b); NO_3 (c); and Cl (d).

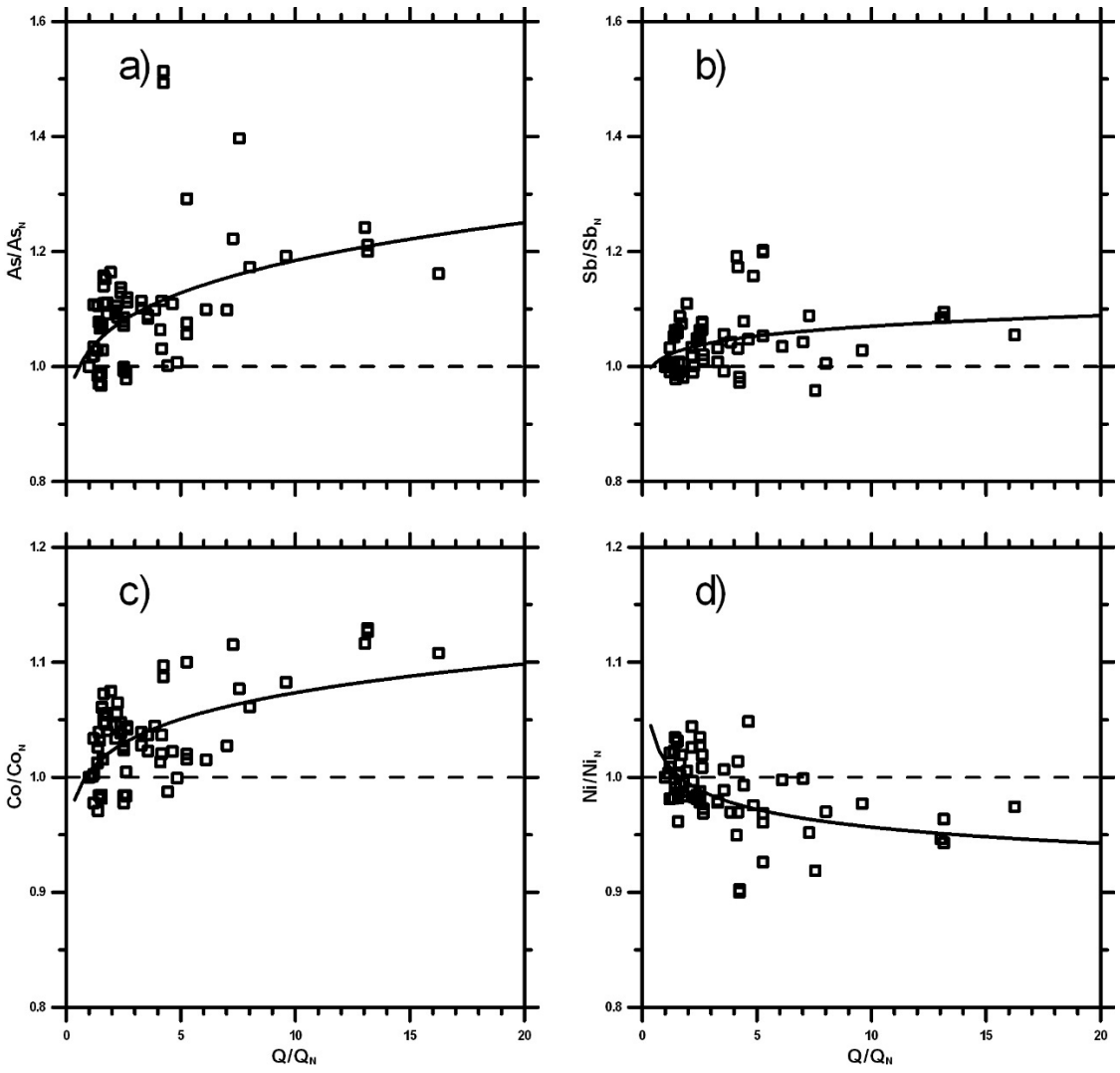

Figure 42: Concentration-Discharge (C-Q) relationships and fitted power-law models for As (a); Sb (b); Co (c); and Ni (d).

The C-Q relationship for SiO_2 does not allow for a meaningful power-law representation because it exhibits two distinct trends, as in the cases of $\delta^{18}O$ and Na (Figure 41a). With increasing Q during the freshet, concentrations rise slightly from baseflow values before levelling off. During the fall, with increasing Q, values decrease slightly. The C-Q behaviour of sulfate is chemostatic based on all metrics (Figure 41b). The C-Q relationship for nitrate, like that of SiO_2, exhibits two distinct trends and a power-law model is inappropriate (Figure 41c). During the freshet, concentrations decrease with Q indicating dilution. In the late summer and fall, values increase with Q compared to baseflow levels. Chloride concentrations also exhibit two distinct trends with respect to Q. During the freshet, from April to June values remain close to baseflow levels. During the rest of the year, Cl increases with Q (Figure 41d). The C-Q behaviour of Cl is similar to that of Na, suggesting the influence of road salt as noted previously.

Based on the metrics in Table 15 and the plots in Figures 40 and 41, the C-Q behaviour of major cations and anions falls into two groups. In the first group, Ca, Mg, and sulfate exhibit a simple chemostatic behaviour, with no correlation between their concentrations and Q. Constituents of the second group (Na, K, SiO_2, NO_3, Cl) may be considered to follow a chemostatic behaviour also, based solely on their metrics (Table 15). However, for these species, power-law C-Q models are inappropriate as the data indicate distinct flushing or dilution trends associated with increasing Q during the freshet or during the fall. For example, SiO_2 exhibits subtle flushing and dilution behaviours during the freshet and the fall period, respectively. Nitrate, on the other hand, shows the opposite behaviour with dilution during the freshet and flushing in the fall.

Based only on their CV_C/CV_Q and β metrics (Table 15), the trace elements As, Sb, Co, and Ni would also be characterized as following chemostatic C-Q patterns. However, C-Q data plots (Figure 42) show that, during the freshet, As, Sb, and Co exhibit subtle flushing whereas Ni exhibits dilution. Although Co, Ni, and Sb show these signs of chemodynamic behaviour, it must be emphasized that their concentrations remain very close to baseflow levels. Arsenic concentrations show a stronger but more complex chemodynamic flushing behaviour. The highest As levels are not observed at peak discharge rates but rather at intermediate rates during the recession limb of the freshet (Figure 27), in association with the hypothesized discharge of a slug of old, low-ORP mine water.

The overall chemostatic nature of the Shaft 98 mine water flow system may be explained by buffering around “set point” solute concentrations through a combination of abundant water storage and fast chemical weathering reactions relative to discharge rates (Godsey et al., 2019). Here, baseflow conditions can be thought of as the “set point” for the Shaft 98 system; the mine pool provides a very large storage volume and secondary minerals forming in the workings above the water table represent readily soluble sources of mine water constituents.

5.5 Metal(loid) loadings to receiving waters

Metal(loid) loadings to receiving waters downstream of Shaft 98 can be estimated from discharge rates and weekly water chemistry analyses. Summary statistics for weekly loadings and annualized total loadings are presented in Table 16. A chemograph for weekly As loadings (Figure 43) shows that they are overwhelmingly controlled by the discharge rate. Similar results are obtained for other metal(loids). Given the low variability of concentrations (Tables 12, 15), these results are perhaps not surprising. The chemostatic behaviour of the Shaft 98 mine drainage system indicates that rates of solute mass export are closely proportional to discharge fluxes. While the physical groundwater flow system exhibits a very dynamic response to recharge events, the geochemical system appears highly buffered.

Table 16: Annual metal(loid) loadings and **s**ummary statistics for weekly loadings based on total (unfiltered) concentrations for the one-year sampling period.

	Co	Ni	As	Sb	Zn	Cu
n	52	52	52	52	52	52
Minimum (kg/w)	0.139	0.115	1.055	0.060	0.077	0.025
Maximum (kg/w)	2.521	1.823	20.625	1.026	1.437	0.444
Mean (kg/w)	0.578	0.430	4.701	0.244	0.325	0.103
Std. dev. (kg/w)	0.517	0.360	4.309	0.211	0.293	0.092
Annual (kg/yr)	30.0	22.3	244.4	12.7	16.9	5.4
Flux weighted mean conc. (µg/L)	104	77	844	44	58	19

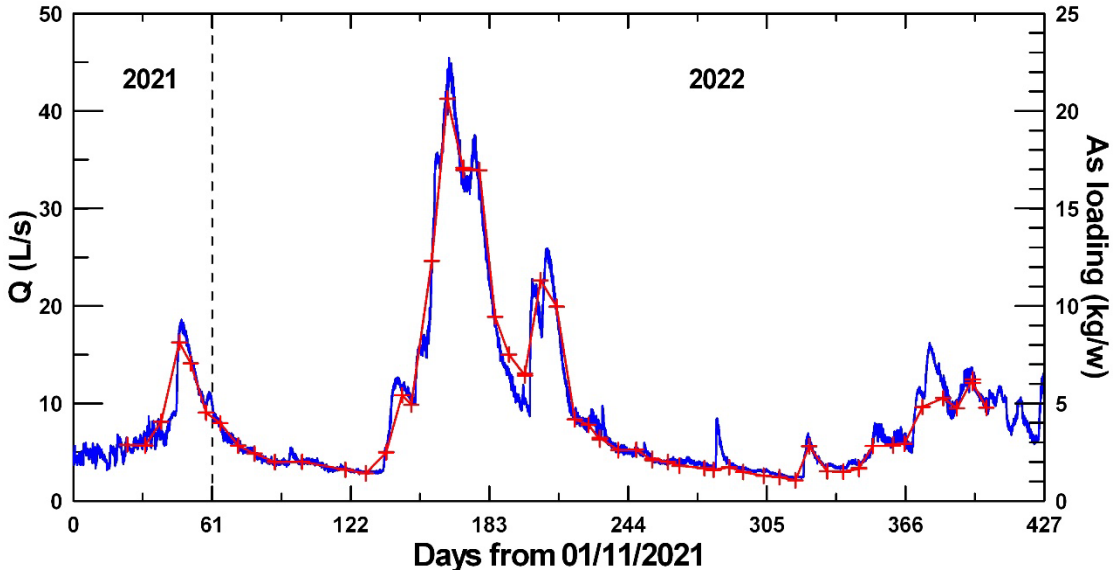

Figure 43: Chemograph of weekly As loading (right scale) with overlay of discharge hydrograph (left scale, in red) from November 1, 2021.

Using arsenic as an example, annual metal(loid) loadings from Shaft 98 can also be estimated using the modeling approach of the previous section. However, the fitted power-law model for As (Figure 42a) has a very low R^2 (Table 15) and is a poor estimator of As concentrations. An alternative approach is to estimate As load (L) directly using the power-law model:

$$L = CQ = \alpha Q^{\beta+1} \quad [3]$$

In the least-squares fitting procedure, this is equivalent to a flux-weighting of concentrations. For As (total) load, the non-linear least-square fit is excellent ($R^2 = 0.991$) as shown in Figure 44.

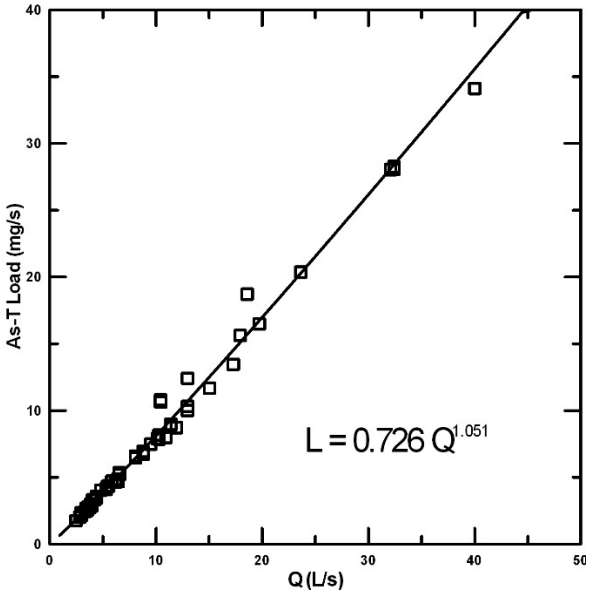

Figure 44: Load of As (total) versus discharge rate showing the non-linear least-squares power-law model fit.

The fitted model for As (total) load can then be used to estimate annual load from Q as recorded by the hydrograph on an hourly basis (Figure 9). The approach yields an annual total arsenic loading from Shaft 98 of 238.4 kg, which is close to the estimate in Table 16 (244.4 kg).

6.0 CONCLUSIONS

With reference to the objectives and scope of this study, the following conclusions can be made:

1. *How does the quantity of mine drainage vary in response to snowmelt and precipitation events?*

During the two-year period of monitoring discharge from Shaft 98, flows varied between 2.1 and 45.4 L/s. The highest flows were observed during the spring freshet, which begins in mid-March and tails off in May. The lowest flows occurred in late summer and early fall, at the end of the hydrological year. Spikes of high discharge were associated with summer convective storms (35 L/s) and late fall rain events (18 L/s). The median flow rate was 6 L/s, and the 95th percentile was approximately 25 L/s.

2. *What are the geochemical characteristics of mine drainage?*

The drainage from Shaft 98 is a circum-neutral (mean pH=7.1) and sub-oxic (mean DO=1.9 mg/L) Ca-HCO_3 type water with moderate dissolved solids content (mean EC = 392 µS/cm). Water stable isotope analyses fall on the local meteoric water line. The drainage has a mean hardness of 188 mg/L $CaCO_3$. Mean sulfate, nitrate, and chloride concentrations are 17.5, 0.87, and 8.4 mg/L, respectively. Some of the chloride is likely derived from road salt. The nitrate may be from a combination of explosive residues in the mine workings and leakage from sewers. Mean dissolved and total Fe concentrations are 55.5 and 130.7 µg/L, respectively. Arsenic (mean dissolved 745.2 µg/L) is the most important metalloid in the drainage. Mean concentrations of dissolved Co, Ni, Sb, and Zn are 98.4, 75.9, 42.2, and 54.3 µg/L , respectively.

3. *How does drainage quality vary with discharge rate?*

Overall, the drainage from Shaft 98 exhibits a remarkably "chemostatic" behaviour, meaning that solute concentrations vary little as a function of discharge rate. Nonetheless, some metal(loid) constituents (As, Co, Sb) show subtle "flushing" (increasing concentrations) with increasing discharge rates whereas others (Ni) show "dilution" (decreasing concentrations). The chemostatic character of the drainage can be attributed to the concentration buffering effect of a large mine pool and to weathering reactions in the exposed workings that are fast compared to solute transport times.

4. *What are the annual metal(loid) loadings from No. 98 Shaft?*

Annual metal(loid) loadings in drainage from Shaft 98 can be estimated from discharge measurements and water chemistry analyses from the quasi-weekly sampling. These loadings are 244.4, 30.0, 22.3, 12.7 and 16.9 kg for As, Co, Ni, Sb, and Zn, respectively. Using the discharge and water chemistry data sets, it is also possible to fit a power-law relationship between metal(loid) loading (L) and discharge rate (Q) by non-linear least-squares regression. This model can then be used to estimate loadings based on continuously monitored Q.

5. *What are the geochemical processes that may control the metal(loid) chemistry of mine drainage?*

On exposed mine workings above the water table, primary arsenide and sulpharsenide minerals are oxidized to form more soluble secondary minerals such as scorodite, pharmacolite, erythrite, and annabergite. These minerals are leached by infiltrating snowmelt and precipitation which mix with older sub-oxic waters in the mine pool. Sorption of As on hydrous ferric oxides (HFO) is limited and most As is transported to the Shaft 98 discharge point in dissolved form. Zinc and Cu also exhibit minor sorption whereas Ag and Pb occur mainly in the suspended particulate phase. Cobalt, Ni, and Sb in mine waters are transported entirely in the dissolved phase.

REFERENCES

Andrews, A.J., Owsiacki, L., Kerrich, R., and Strong, D.F., 1986. The silver deposits at Cobalt and Gowganda, Ontario. I: Geology, petrography, and whole-rock geochemistry; Can. J. Earth Sci., 23, 1480-1506.

Berry, L.G. (editor), 1971. The silver-arsenide deposits of the Cobalt-Gowganda region, Ontario. Can. Mineral., 11, Part 1, p.1-430

Boyle, R.W. and Dass, A.S., 1971. The geochemistry of the supergene processes in the native silver veins of the Cobalt - South Lorrain area, Ontario. Can. Mineral., 11, Part 1, The silver-arsenide deposits of the Cobalt-Gowganda region, Ontario, 358-390.

Brakensiek, D.L., Osborn, H.B., and Rawls, W.J., 1979. Field Manual for Research in Agricultural Hydrology. Agriculture Handbook 224, U.S. Dept. of Agriculture, 550 pp.

Brooks, P.D., Chorover, J., Fan, Y., Godsey, S.E., Maxwell, R.M., McNamara, J.P., and Tague, C., 2015. Hydrological partitioning in the critical zone: Recent advances and opportunities for developing transferable understanding of water cycle dynamics. Water Resour. Res., 51, 6973-6987; doi:10.1002/2015WR017039.

Dumaresq, C. G., 1993. The occurrence of arsenic and heavy metal contamination from natural and anthropogenic sources in the Cobalt area of Ontario. M.Sc. thesis, Dept. of Earth Sciences, Carleton University, Ottawa, Ontario, 309 pp. (electronic version, 2005)

Dumaresq, C.G. 2023. Cobalt Mining Legacy; website accessed may 2023; http://www.cobaltmininglegacy.ca/index.php

Clarke, J., 2017. The characterization of arsenic mineral phases from legacy mine waste and soil near Cobalt, Ontario. M.Sc. thesis, Dept. of Geological Sciences and Geological Engineering, Queen's University, Kingston, ON, 100 pp.

Environment Canada, 2001. Guidance Document for Flow Measurements of Metal Mining Effluents – Final Report. EPS/MM/4, April 2001, Minerals and Metals Division, Environmental Protection Service, Environment Canada, Ottawa.

ECCC, 2023. Canadian Climate Normals, Environmental and Climate Change Canada; website accessed in May 2023; http://climate.weather.gc.ca/climate_normals

ESWG, 1995. A National Ecological Framework for Canada. Ecological Stratification Working Group, Agriculture and Agri-Foods Canada, Research Branch, Centre for Land and Biological Resources Research and Environment Canada State of the Environment Directorate, Ecozone Analysis Branch, Ottawa/Hull; Report and national map at 1:7 500 000 scale; Canadian Council on Ecological Areas website accessed May 2023; http://ecozones.ca

EWG, 1989. Ecoclimatic Regions of Canada, First Approximation. Ecoregions Working Group of the Canada Committee on Ecological Land Classification; Ecological Land Classification Series 23, Can. Wildlife Service, Environment Canada, Ottawa, 119 p. and map at 1:7 500 000 scale; report accessed May 2023; https://publications.gc.ca/site/eng/9.867547/publication.html

Godsey, S.E., Kirchner, J.W., and Clow, D.W., 2009. Concentration-discharge relationships reflect chemostatic characteristics of U.S. catchments. Hydrol. Processes, 23, 1844-1864; https://doi.org/10.1002/hyp.7315

Godsey, S.E., Hartmann, J., and Kirchner, J.W., 2019. Catchment chemostasis revisited: Water quality responds differently to variations in weather and climate. Hydrol. Processes, 33, 3056-3069; DOI: 10.1002/hyp.13554

Grant, D.M. and Dawson, B.D., 1997. ISCO Open Channel Flow Measurement Handbook, 5th edition. ISCO Environmental Div., Lincoln, Nebraska, 501p.

Gwinn, W.R. and Parsons, D.A., 1976. Discharge Equations for HS, H, and HL Flumes. Jour. Hydraulics Div. ASCE, 73-88, January 1976.

Hall, F.R., 1970. Dissolved solids-discharge relationships: 1. Mixing models. Water Resources Res., 6(3), 845-850; https://doi.org/10.1029/WR006i003p00845

Hall, F.R., 1971. Dissolved solids-discharge relationships: 2. Application to field data. Water Resources Res., 7(3), 591-601; https://doi.org/10.1029/WR007i003p00591

Jambor, J.L., 1971a. General geology. Can. Mineral., 11, Part 1, The silver-arsenide deposits of the Cobalt-Gowganda region, Ontario, 12-33.

Jambor, J.L., 1971b. Gangue mineralogy. Can. Mineral., 11, Part 1, The silver-arsenide deposits of the Cobalt-Gowganda region, Ontario, 232-262.

Jambor, J.L., 1971c. Wall rock alteration. Can. Mineral., 11, Part 1, The silver-arsenide deposits of the Cobalt-Gowganda region, Ontario, 272-304.

Knight, C.W., 1924. Geology of the Mine Workings of Cobalt and South Lorrain Silver Areas. Ontario Department of Mines, Annual Report 1922, vol.31, Part 2, p.1-238.

Lottermoser, B.G., 2011. Recycling, reuse, and rehabilitation of mine wastes. Elements, 7, 405-410; DOI: 10.2113/gselements.7.6.405

Maher, K., and Chamberlain, C.P., 2014. Hydrologic regulation of chemical weathering and the geologic carbon cycle. Science, 343, 1502-1504; https://www.science.org/doi/10.1126/science.1250770

Markl, G., Marks, M.A.W., Derry, I., and Guhring, J.-E., 2014. Weathering of cobalt arsenides: Natural assemblages and calculated stability relations among secondary Ca-Mg-Co arsenates and carbonates. Amer. Mineral., 99, 44-56; http://dx.doi.org/10.2138/am.2014.4540

Miller, W.G., 1913. The cobalt-nickel arsenides and silver deposits of Temiskaming. Ontario Department of Mines, Annual Report, vol. 19, Part 2, pp. 1-133.

Moore, R.D., 2005. Introduction to salt dilution gauging for streamflow measurement Part III: Slug injection using salt in solution. Streamline Watershed Management Bulletin, 8(2), 1-6; http://library.nrs.gov.bc.ca/digipub/Streamline%20V08N02.pdf

Musolff, A., Schmidt, C., Selle, B., and Fleckenstein, J.H., 2015. Catchment controls on solute export. Adv. Water Resources, 86, 133-146; http://dx.doi.org/10.1016/j.advwatres.2015.09.026

OCF, 2023. Open Channel Flow website; accessed May 2023. https://www.openchannelflow.com/blog/h-flume-flow-equation-and-tables

Petruk, W., 1971a. General characteristics of the deposits. Can. Mineral., 11, Part 1, The silver-arsenide deposits of the Cobalt-Gowganda region, Ontario, 76-107.

Petruk, W., 1971b. Mineralogical characteristics of the deposits and textures of the ore minerals. Can. Mineral., 11, Part 1, The silver-arsenide deposits of the Cobalt-Gowganda region, Ontario, 108-139.

Petruk, W., Harris, D.C., and Stewart, J.M., 1971a. Characteristics of the arsenides, sulpharsenides, and antimonides. Can. Mineral., 11, Part 1, The silver-arsenide deposits of the Cobalt-Gowganda region, Ontario, 150-186.

Petruk, W., and staff, 1971b. Characteristics of the sulphides. Can. Mineral., 11, Part 1, The silver-arsenide deposits of the Cobalt-Gowganda region, Ontario, 196-231.

US Environmental Protection Agency – EPA, 2001. Performing Quality Flow Measurements at Mine Sites. Report EPA/600/R-01/043, Office of Research and Development, Washington DC 20460.

WSC, 2023. Water Survey of Canada, Historical hydrometric data. Website accessed May 2023; https://wateroffice.ec.gc.ca/

Sergiades, A.O., 1968. Silver Cobalt Calcite Vein Deposits of Ontario. Ontario Department of Mines, Mineral Resources Circular No. 10, 498p.

SRK Consulting (2016). Metal leaching and acid rock drainage characterization of tailings from Agnico Eagle Mines Ltd. Properties in the Cobalt/Coleman Area, Ontario – 2016 Update – Final; report prepared for Story Environmental Inc. and Agnico Eagle Mines Ltd., 129pp.

Thompson, M. and Howarth, R.J., 1978. A new approach to the estimation of analytical precision. Jour. Geochem. Explor., 9, 23-30.

Thompson, S.E., Basu, N.B., Lascurain Jr., J., Aubeneau, A., and Rao, P.S.C., 2011. Relative dominance of hydrologic versus biogeochemical factors on solute export across impact gradients. Water Resour. Res., 47, W00J05; doi:10.1029/2010WR009605

Thomson, R., 1957. Cobalt camp; In: Structural geology of Canadian ore deposits, Proceedings of the 6th Commonwealth Mining and Metallurgical Congress. Can, Inst. Min. Metall., Special Vol. 2, pp. 377-388.

Walker, T.L., 1924. Chapmanite, a new hydrous ferrous silico-antimonate from South Lorraine, Ontario. Univ. of Toronto Studies, Geol. Ser., 17, 5-8.

Wymore, A.S., Larsen, W., Kincaid, D.W., Underwood, K.L., Fazekas, H.M., McDowell, W.H., Murray, D.S., Shogran, A.J., Speir, S.L., and Webster, A.J., 2023. Revisiting the origins of the power-law analysis for the assessment of concentration-discharge relationships. Water Resour. Res., 59, e2023WR034910; https://doi.org/10.1029/2023WR034910

APPENDIX 1

Figures A-1 and A-2

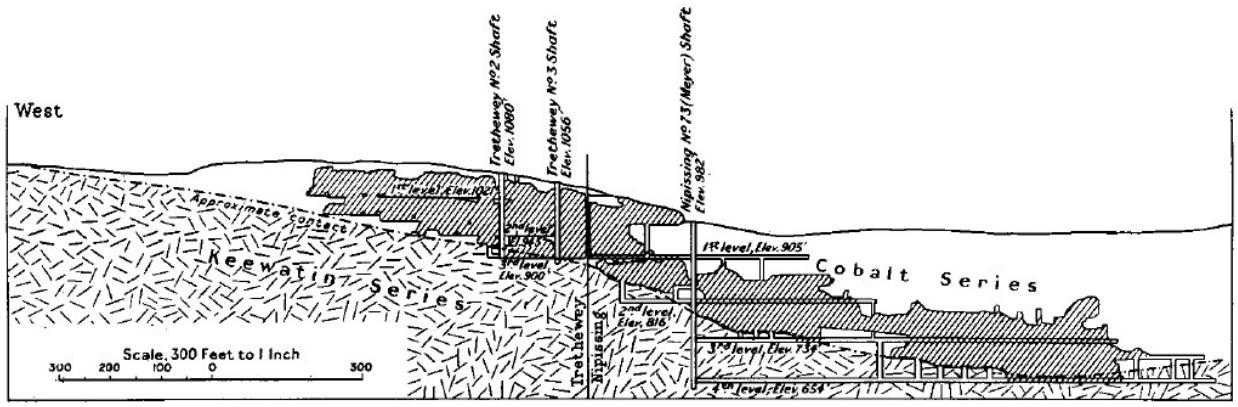

Fig. 5—Stope section on the Meyer vein of the Nipissing and the "main" vein on the Trethewey. The ore-shoot has a length of about 1,600 feet. The ore occurs almost entirely in the Cobalt series. On the Nipissing, the ore-shoot only rises above the Keewatin an average height of about 110 feet; above the stope the vein is a barren calcite vein about three-quarters of an inch wide. . Stope sections furnished by the Nipissing and Coniagas.

Figure A-1: Longitudinal section along the Meyer vein and its western extension on to the Trethewey property showing the location of stopes above the contact between the Archean "Keewatin" series and the Coleman member of the Proterozoic Cobalt series. The location of Shaft 98 is not shown on this section. However, it is approximately 300 m (1000 ft) east of the No. 73 (Meyer) shaft, and its collar elevation is 14.9 m (49 ft) lower. Reproduced from Knight (1924).

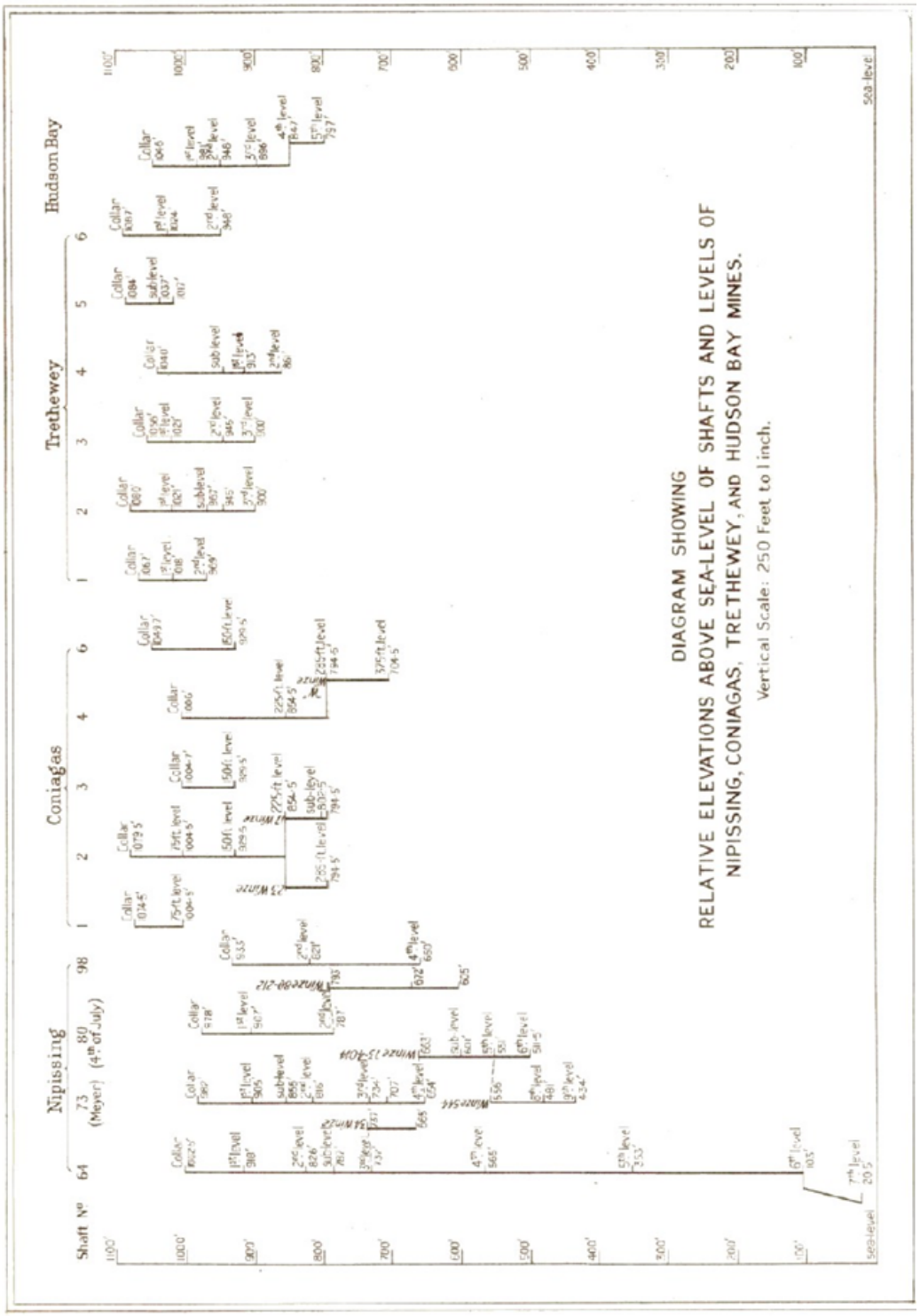

Figure A-2: Diagram showing the relative elevations of shaft collars and mine working for the Nipissing, Coniagas, Trethewey, and Hudson Bay mines. Reproduced from Knight (1924).

APPENDIX 2

Water Sampling Protocol for the Shaft 98 Study

WATER SAMPLE COLLECTION AND STORAGE

1) Before heading out to sample: calibrate the YSI multi-parameter instrument as follows: calibrate Electrical Conductivity (EC) using an appropriate standard solution; calibrate pH using pH=7 buffer solution (first) and pH=10 buffer solution (second); calibrate dissolved oxygen (DO) and check redox potential (ORP) as per instrument instructions.
2) Before heading out to sample: pre-label 60 mL HDPE sample bottles as follows: dissolved cations, filtered and acidified (marked C+ and FA); total cations, unfiltered and acidified (marked C+ and UA); anions, filtered and *unacidified* (marked A- and FU); stable isotopes (marked isotopes); Indicate the date and approximate time of sampling; Bring spare syringes, filters and sample bottles.
3) At Shaft #98: Remove any debris from flume if necessary; Measure stage in flume; Record temperature, EC, pH, DO, ORP of discharge water in the central stream of the flume.
4) At Shaft #98: Before sampling, rinse new syringe three times with water to be sampled. Water samples are to be taken from the corrugated culvert immediately upstream of the flume.
    a) **Unfiltered Cation Samples:** Using syringe, rinse the total cations (C+ UA) sample bottle three times (10-20 mL per rinse) from the water to be sampled; fill the bottle so that the meniscus bulges above the rim and no air is trapped inside; Seal tightly.
    b) **Filtered Cation Samples:** Fill syringe with water; Place a filter capsule on the end of the syringe (do not touch the tips of the syringe or filter with your hands, handle from the sides only). Pushing on the plunger, discard the first 10 mL of sample through the filter; Using the rest of the water through the filter, rinse the dissolved cations (C+ FA) sample bottle three times; shake vigorously and discard rinse water thoroughly. To fill the bottle, temporarily remove the filter (taking care not to touch tip) and fill syringe from water to be sampled; Replace the filter and depress plunger slightly to discard a few drops of water before filling the (C+ FA) bottle; Fill so that the meniscus bulges above the rim and no air is trapped inside; Seal tightly.
    c) **Filtered Anion Samples:** Repeat the triple rinsing, filtering and filling for the anions (A- FU) sample bottle. Change filters as soon as it gets hard to push the syringe plunger. If you need to replace the filter (it may get clogged), remember to rinse filter with the first 10 mL of sample. Fill the anions (A- FU) bottle to the top as above, leaving no airspace, and seal tightly.
    d) **Stable isotope Samples:** Fill the sample bottle as for the filtered anion samples.
5) Store water sample bottles under cool and dark conditions, in a refrigerator, pending shipment to the GSC laboratory. Do not allow bottles to be immersed in ice water; store in plastic bags, by batch, and keep dry.
6) NOTE: Samples will be acidified on arrival at the GSC laboratory

CONTROLS - BLANKS AND DUPLICATES

Sample blanks

For a sample blank, prepare a 60 mL bottle of DDI water as you would a filtered and acidified water sample. This type of control will highlight any contamination problems associated with the sample preparation procedure. To prepare a sample blank: Transfer enough DDI water from the "mother" container (Supplied by the GSC) to a collection bottle after rinsing it. *Do not use a previously used collection bottle, except one that is reserved for DDI water only.* Using a fresh filter and syringe, rinsed as per instructions, fill a 60 mL sample bottle marked "SB – FA" (Sample Blank- filtered and acidified) from the collection bottle. Prepare one sample blank per batch of samples shipped to the GSC lab, i.e. every four weeks.

Duplicate field samples

A duplicate field sample is just like a regular water sample. It is used to flag accidental contamination during the sampling process and to verify reproducibility of results. To prepare a duplicate sample, simply fill four additional 60 mL sample bottles marked "DUP C+UA" (Duplicate, cations, unfiltered and acidified), "DUP C+ FA" (Duplicate, cations, filtered and acidified), "DUP A- FU" (Duplicate, anions, filtered and un-acidified) and "Isotopes", as per usual procedure. Do this once every four weeks, for a random sampling day.

In summary, every four weeks, you will ship to the GSC laboratory in Ottawa a cooler (with freeze packs) containing the following:

- 16 60 mL sample bottles corresponding to four sets of four bottles from four weekly sampling days at the Shaft #98 site. In addition to date, the three bottles in each set are marked "C+ FA", "C+ UA", "A- FU" and "Isotopes". Number samples consecutively by sampling day using the GSC officer code for 2021 (DUA-21) as a prefix. Thus, DUA-21-01 for the first set, DUA-21-02 for the second set, and so on.
- 4 60 mL sample bottles marked "DUP C+UA", "DUP C+ FA", "DUP A- FU", "Isotopes" on a randomly selected sampling day, and assigned a sample number in the normal sequence.
- 1 60 mL Sample blank bottle marked "SB – FA"